Formation of protective lubricious oxide layers on the surface of nitrogen alloyed steels in self-mated sliding

Bildning av skyddande smörjande oxidskikt på ytan hos kvävelegerade stål vid självmatad glidande kontakt

Amin Aeyadi

Faculty of health, science and technology

Degree project for master of science in engineering, mechanical engineering

30 credit points

Supervisor: Pavel Krakhmalev

Examiner: Jens Bergström

Date: Spring semester 2015, 2015-06-29-

Abstract

In most of our machining applications we attend to use lubricants to prevent direct metal-metal contact between the tool and the work piece, but in many cases still the metal-metal contact happens due to a number of reasons as high contact loads, low viscosity, lubrication characteristics lose (physical and/or chemical), inefficient lubricant distribution systems, etc. In such situations the metal-metal contact might result in extreme and unexpected wear caused by adhesion, abrasion, oxidation, etc. Some tool materials in some certain conditions generate different types of low friction protective tribo-layers such as Magneli phases or tribo-oxides over the contact surfaces.

We ran the experiments using a block-on-cylinder lab test machine in room temperature and measured the friction force in the contact area with a load cell. We also used SEM and EDX to analyze the chemical composition of the contact surface of the blocks plus the material (debris) which was removed from the contact surfaces and piled up over a small area at the end of contact surface of the test samples. We finally measured the worn area (which is a relative indication of the worn volume) with OM.

Our test materials were three different PM tool steels (Vancron 40 and Vancro 50 wich are nitrogen alloys and Vanadis 10 nitrogen free alloy) all produced by UDDEHOLM company in Sweden, in self mating sliding tests to compare the influence of the alloying elements and hard phases on wear resistance and the composition and characteristics of the tribo-layers. The hardness of the three test materials are close to 64 HRC with different hard phase compositions.

On one hand presence of some elements in chemical composition of the tool steels may cause the capability to generate the protective oxide phases. The environmental and physical conditions play critical roles in this regard as well. By this experiment we found that however these materials fulfill the chemical requirements to create protective low-friction tribo-layers, due to insufficient temperature; they are unable to generate protective trio-layers in large scales.
On the other hand the microstructural components as carbide and nitride hard phases have great influence on the wear resistance and friction rate of the mating materials. Here we also see that the load is not a critical factor for the wear rates. And also that the amount of Nitrogen content in the alloys has direct effect on the wear rate.

Contents

1. Introduction

1.1 Steels

Steels are namely defined as alloys composed of iron and other elements. In many literatures small amount of carbon is mentioned as a main part of steels besides other elements. Therefore the steels without carbon are traditionally called iron and steels containing carbon are considered as carbon steels.

Carbon steels are categorized in four major groups:

- Plain carbon steels; for bar and forging applications with definite ranges carbon, max.1.65% Mn, max.0.60% Cu, S & P.
- Alloy steels; with definite ranges carbon, Mn, Cu, Si, S & P, but may also contain Al, Cr, Co, Nb, Mo, Ni, Ti, V, W, Zr, etc.
- Stainless steels
- Tool steels
  These last two groups of steels are more heavily alloyed than carbon steels and alloy steels.

1.2 Alloying elements

Carbon forms carbides and graphite which is more stable form of carbon than iron-carbide.

By increasing the carbon and silicon contents in tool steels, graphite formation is promoted which will improve the machinability. Also boron nitrides have been found to be effective in graphite nucleation in medium-carbon steels.

The steel processing is based on the existence of austenite phase therefore this science tries to control the transformation of austenite to other phases on cooling process which is the main object in achieving a great variety of micro structures and properties through heat treatments. So we see all hot working of heavy sections are applied at temperatures where austenite is stable phase.

Carbon is a main element which stabilizes the austenite phase in steels. But there is a limit on solubility of carbon in steels which is Maximum 2.11% in austenite and considerably less in ferrite. By exceeding the amount of carbon from this limit, a new phase forms which is called iron carbide or cementite which is a hard phase.

Small amounts of chromium to Fe-C alloys will cause M3C cementite structure; larger amounts will provide M7C3; and still larger portions produce M23C6.

Some elements like manganese, carbon, nitrogen and nickel are austenite stabilizers and lower the eutectoid temperature; silicon, chromium and niobium are ferrite stabilizers and enlarge the ferrite phase field; and titanium, tungsten, vanadium, manganese, niobium, molybdenum and chromium are carbide formers.

Almost all of the alloying elements cause the formation of pearlite to be reduced due to their sluggish diffusion and in fact this effect is desired in heat treatments [1].

High nitrogen alloyed systems with dense hard phase and low friction properties show improvements in performance where galling and cold welding or adhesion forces us to replace the tools early, this material gives considerable improvements in powder pressing, cold forming, cold rolling and cutting which are metal working applications and also in plastic applications where adhesion and sticking cause a lot of maintenance. In general, steels with more hard phases (carbides and nitrides) with more even distribution show better wear resistance than the steels with soft carbides. [2]

1.3 Back grounds

1.3.1 TOOL STEELS

Tool steels are the steels used to form, cut, grind and machine other materials therefore are designed to have considerable high hardness and durability under severe service conditions.

These steels are manufactured in higher complexity such as cooling rates, heat treatment time and temperature, etc and they are in fact more heavily alloyed and are achieved a proper balance of alloy carbides in a matrix of martensite but actually their heat treatment is partially similar to that of the hardenable low alloy steels as austenitizing, martensite forming and tempering. Tool steels are designed largely based on strong carbide-forming elements such as chromium, molybdenum, tungsten and vanadium.

The wear resistance of tool steels increases by raising the fraction of carbide phases [1].

While carbon based high chromium steel grades having high mechanical properties as hardness and wear resistance still are not proper for some certain environments regarding their corrosion resistance properties. Achieving a higher corrosion resistance with high wear resistance relies on significant increase in hard phase carbides which is a quite difficult process.
There is still one other option to increase the corrosion resistance and at the same time achieving higher hardness and high rate of hard phase carbide for a proper wear resistance by replacing carbon by nitrogen. This is a process based on powder metallurgy which ends in developing new grades of steel with unique properties with high corrosion resistance, hardness, wear resistance, and low friction [2].

1.3.2 Powder Metallurgy Tool Steels

The P/M method was first introduced and used to manufacture advanced high-speed tool steels, however later was found to be a proper method for cold-work and hot-work tool steels manufacturing. With this method several essential properties have been improved in tool steels; properties as machinability, grindability, dimensional control during heat treatment, cutting performance, etc. It also offers a better toughness and ductility for cold-work tooling and better thermal fatigue life and toughness for hot-work tooling [1, 3].

1.4 Wear mechanisms and wear protective tribo-layers

1.4.1 Oxidation and oxidational wear

According to Quinn's oxidational wear parabolic theory which was introduced based on diffusion law; 1-3 μm is the critical thickness for oxide to break up and appear as wear debris, this wear is considered as mild-wear. To predict the wear rate of metals in sliding conditions, Quinn developed a model based on the earlier mentioned theory. [4-7] Later on two other tribologists defined a mild-oxidational wear at sliding speed range of 0.6-60 m/s so that when the sliding speed exceeds this range the wear mechanism becomes severe-oxidational wear. [8]

The oxidation starts in a very short time after the surfaces start sliding against each other. So, Yu and Chuang set up a test to estimate a rate for this phenomenon, and they saw that after a short time like 10 seconds only a small part of the nominal contact surface was covered with oxide films. The longer the test went on the larger area were covered by oxide film correspondingly, but also depending on sliding speed and normal load. [9]

The dominant oxides in tool and die steels are Fe2O3 which forms in low load and low sliding speed conditions, FeO which forms in medium to high loads and speeds and Fe3O4 which is often found in conditions in between two initial conditions. [10]

The oxide films are not of the same thickness all over the contact surface, this character is proportional to the depth of plastic zone. This might indicate that the temperatures in plastic zones are higher than in elastic zones. Moreover there are many defects for oxygen to diffuse easily. [11]

The oxide films over the contact surface subjected to the robbing crack and spall off resulting in mass loss from the mating materials. Normally the oxide films do not break up and spall off all at once, and this happens gradually and partially. [6, 9-12]

Sliding speeds below 1m/s normally do not generate a sufficient flash temperature over the contact point to make the oxidation the dominant wear mechanism. This thin but hard oxide layer separates the surfaces and prevents the direct metal to metal contact in relatively low loads. In such situations fine oxide particles are generated and mild wear is caused [13, 14]. These fine particles can come from the removed and oxidized metallic debris. The damaged surfaces deoxidize again and prevent direct metallic contact and causing the continuous mild wear condition [15].

By increasing the sliding speed over 1m/s the flash temperature due to friction rises considerably so that the oxidation rate of the contact zone increases. Therefore the oxidation becomes a dominant wear particle generating mechanism. Here the oxidational wear may form two different wear characteristics including mild-wear and severe-wear [8].

1.4.1.1 Mild-oxidational wear

At the sliding speeds over 1m/s the flash temperature create thick and brittle oxide films appearing as islands over the sliding surface [16]
By having sufficient load to penetrate these oxide films on a soft substrate, break and remove them, the direct metal-metal contact occurs so that the severe wear happens over the sliding surface.
With increasing the load and speed, the flash temperature raises causing formation of a hard surface layer as martensite simultaneous with the local oxidation rate increase resulting in thicker and more uniform distribution of oxide film supported by the hard material underneath which prevents the metal-metal contact, causing a considerable wear rate reduction [17, 18].

1.4.1.2 Severe-oxidational wear

Increasing the speed (over about 10m/s) will cause the oxide layer to change from small separate patches over the sliding surface to plastically deformed uniformed films covering the sliding surfaces [19-21]. Such conditions generates thicker, more unified oxide layers compare with mild-oxidational wear and hotter and more plastic oxides compared with brittle nature of colder oxides, the wear rates are lower and the resulting in more severe sliding conditions [8].

1.5 PM tool steels wear

The investigations of the surface state and micro-hardness results showed that the dominant oxidational wear is observed in wide load range for “hard” specimens, while some competing wear mechanisms are operated under the same values of p for “soft” specimens [22].

High friction, gross seizure, and severe wear are the results of the hard metals sliding on hard metals without liquid lubricant as in steel against steel. This kind of sliding is in use in industry and machinery as in wheels and rails, brakes, clutches, piston rings, rollers, etc [23]. However mild abrasive wear is namely a dominant wear mechanism of PM tool steels, adhesive wear (as galling) also occurs [24-26].

By investigating two different types of PM tool steels manufactured by UDDEHOLM , one alloyed with nitrogen and the other one alloyed without nitrogen, the investigators observed that the one with nitrogen shows 20 times longer life time than the one without nitrogen. The dominant wear mechanism for the nitrogen free alloy was reported to be severe galling while for the nitrogen alloy it was mild abrasive wear. [27].

1.5.1 Magneli Phase; low friction oxide

Magneli phase is titled to ‘’homologous series’’ of Molybdenum, Tungsten, Vanadium, Titanium and Niobium oxides in crystal structure (M_nO_{3n-1} and M_nO_{3n-2}) introduced by Magneli in 1953. Vanadium Pentoxide (V_2O_5) and Vanadium dioxide (VO_2) do not follow the above regularities for structure but are having characteristic similarities [28-32].

Due to the existence of crystallographic shear planes (oxygen deficient layers which increase shearing) in crystal structure of the vanadium Magneli phases; they cause considerable

reductions in friction coefficient [33, 34]. Vanadium Magneli phases were appeared over the contact surfaces of the samples in temperatures over 500°C and in that temperature range they appear to be very effective in decreasing the friction rate [33-37].

In the present research, we propose to conduct tests of selected N-alloyed PM steels in self-mate contact under selected conditions as load, sliding distance, etc at the room temperature. Of the special interest will be critical conditions if a continuous protective layer is formed and what is a chemical composition and phase constitution of this layer. We will investigate the wear mechanisms. We will investigate the influence of Nitrogen content and hard phases.

2. Methodology

2.1. Materials

The wear tests were carried out on a 'block-on-cylinder' testing machine. The composition of the test blocks of 5 x 10 x 20 which slide on cylinders of Ø100mm with the same material are given in the Table1.

	C	N	Cr	Mo	W	V	Mn	Si	Hard Phases
Vancron50	1.1	2.6	4.5	2.3	0.6	12	0.5	0.5	19%MN
Vancron40	1.1	1.8	4.5	3.2	3.7	8.5	0.4	0.5	14%MN+5%M6C
Vanadis10	2.9	-	8	1.5	-	9.8	0.5	-	16%MC+7%M7C3

Table1: Chemical composition of steels used for investigation (wt %)

The Surface finish of the blocks are fine grinded and polished.

The steel Vanadis10 (S1) was Austenitized at 1020° Celsius for 30 minutes, Quenched in Vacuum bath for 100 minutes and Annealed at 525° Celsius for 2 x 2 minutes (2 min. at each stage). The final result is hardness of 64.0 HRC.

The steel Vancron 40 (S2) was Austenitized at 1020° Celsius for 30 minutes, Quenched in Vacuum bath for 100 minutes and Annealed at 560° Celsius for 3 x 1 minutes (3 min. at first stage and 1 min. at second stage). And the final result is hardness of 64.3 HRC.

The steel Vancron 50 (S3) was Austenitized at 1020° Celsius for 30 minutes, Quenched in Vacuum bath for 100 minutes and Annealed at 560° Celsius for 3 x 1 minutes (3 min. at first stage and 1 min. at second stage). And the final result is hardness of 64.1 HRC.

All the wear tests carried in the room temperature, same sliding speed for all the tests which are similar as in SOFS or real deep drawing conditions (lubricated), three different loads and three different lubrication conditions as follows.

2.2 Test Equipment

The hot-wear block-on-cylinder lab-test machine (Figure 1) situated at KaU were used for wear tests. During the test a rectangular wear sample (Test Sample) was mounted in a sample holder equipped with a hemispherical insert ensuring proper contact between the test sample and a steel cylinder (Test Cylinder) rotating at a constant speed. The wear surface of the sample was perpendicular to the loading direction. Double lever system was used to press the sample to the ring with a constant load (P). The pressing load was measured by a load cell (Load Cell 1) with an accuracy of 2% and the friction force between the test sample and the cylinder (F) was measured by another load cell (load Cell 2) with the same accuracy as Load Cell 1. Specimens were tested at selected load and duration at room temperature.

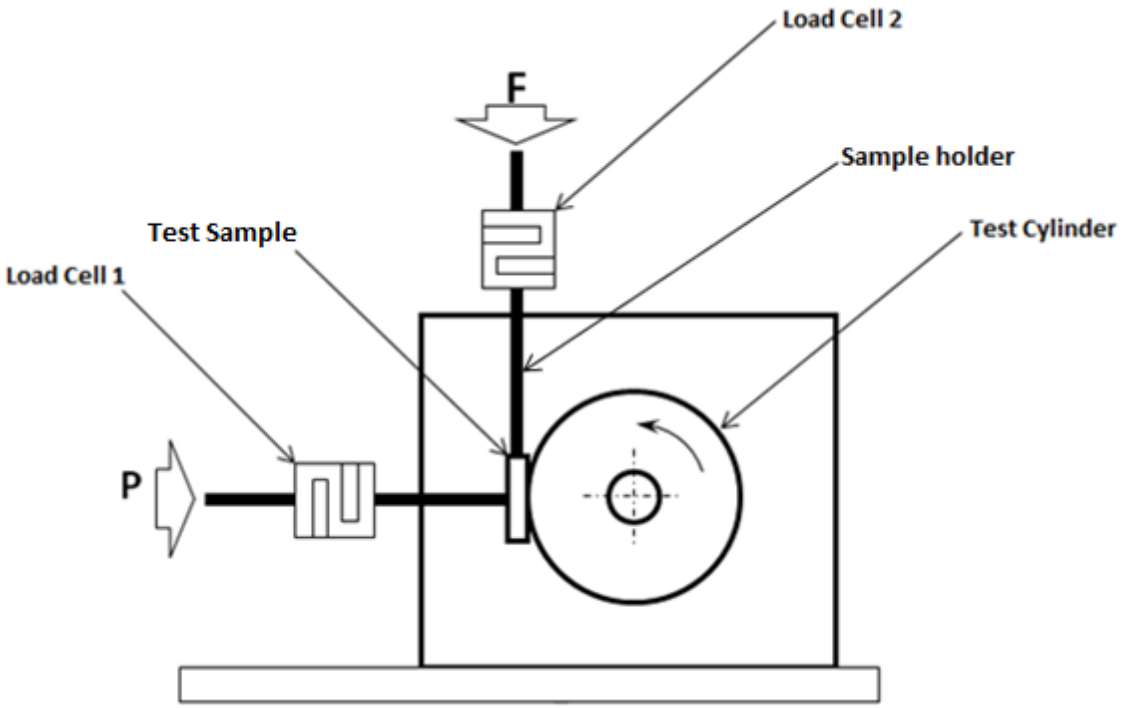

Figure 1: Tribo-system; wear test principle

SEM/ EDX and OM equipments were used to characterize the tribo-layer, debris and worn area/.volume. Wear rates and friction coefficients were evaluated as well.

2.3 Lubrication

- Full-lubrication: the cylinders surfaces were covered by lubricant and lubricated constantly during the tests (Figure 2).

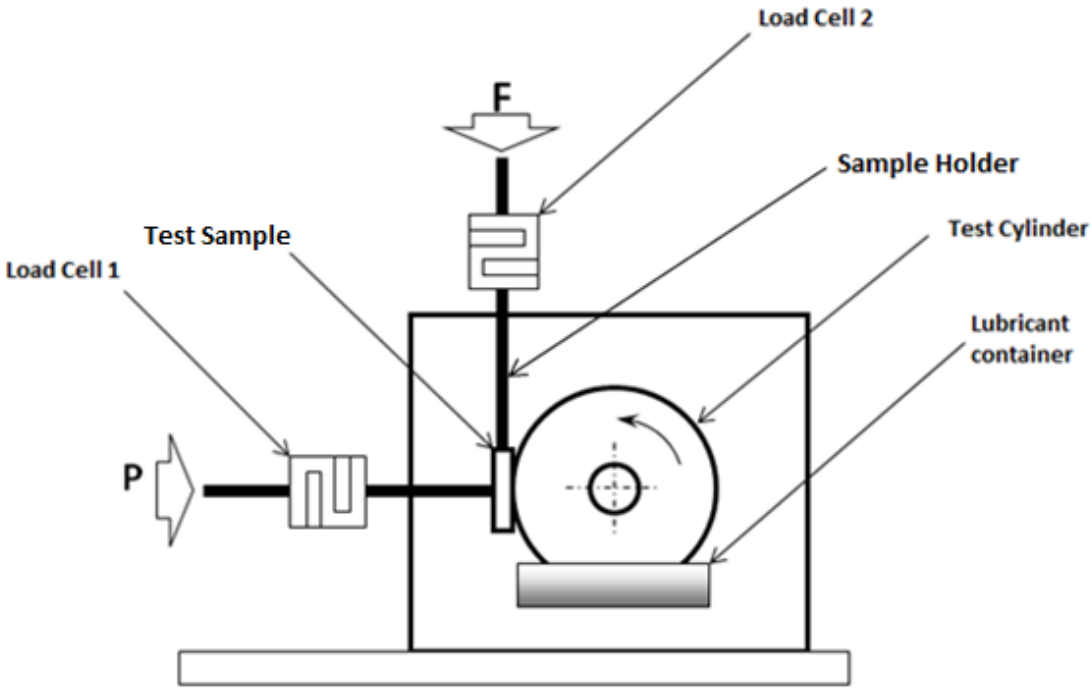

Figure 2: Tribo-system; full-lubrication principle

- Poor/Semi-lubrication: the surfaces were covered by the lubricant once at the beginning of the test but were not renewed later during the tests.
- Dry/Non-lubrication: at this level both the surfaces of the block and the cylinder were directly in contact with each other and exposed to the air.

2.3.1 Lubricant

- The lubricant we used for the tests is Shell Ondina Oil 927 which is a highly refined, non-stabilized, aromatic-free paraffinic white mineral oil with characteristics as mentioned in the Table2.

Colour (Saybolt)	ASTM D 156	+30
Density at 15 °C Kg/m³	ISO 12185	865
Refractive Index at 20 °C °C	ASTM D 1218	1.473
Flash point COC °C	ISO 2592	205
Pour Point °C	ISO 3016	-21
Dynamic Viscosity at 20 °C mPa*s	ISO 3104	72
Kinematic viscosity At 20 °C mm²/s At 40 °C mm²/s At 100 °C mm²/s	ISO 3104	 83 31 5.1
Sulphur (X-Ray) %m/m	ISO 14596	< 0.001
Carbun Type Distribution C/A (S-corr.) C/A (S-corr.) % C/A (S-corr.) %	DIN 51378 / ASTM D 2140 Mod.	 38 62
Refractive Intercept (RI)	DIN 51378	1.0425
Viscosity Gravity Constant (VGC)	DIN 51378	0.809
Aniline Point °C	ISO 2977	107

Table2: Typical Physical Characteristics of the Shell Ondina Oil 927

2.4 Loading

We run the tests with three different load ranges for each material as follows:

- 470N
- 370N
- 270N

2.5 Sliding speed

The sliding speed was constant and the same for all the tests and regarding the 80 RPM on the turning machine the sliding speed can be calculated as follows;

$$Sliding\ speed = r.\omega$$

r: radius of the cylinders (50mm = 0.05m)

ω: Angular speed in Radian ($\omega = 2.\pi.rpm = 2.\pi.60 = 376.9\ Rad/m$in

$sliding\ speed = 0.05 \times 376.9 = 18.8\ m/min$

The test period was planned to carry on for max. 25 minutes but in some cases especially at dry conditions with highest load by sudden extreme rise in CoF which was a sign of initiation of seizure (severe wear) the test was aborted unconcerned about the sliding distance.

The wear rate of the blocks is estimated by measuring the contact area on the block surfaces, the bigger the contact area is the more material removed from the surface. The worn surface areas were measured by an OM..

3. Results

3.1 Friction test results

During these tests the temperatures were registered as follows:

1. High load
   - Dry: Approx. 125 degrees Celsius
   - Poor lubrication: Approx. 60 degrees Celsius
   - Continuous lubrication: Approx. 50 degrees Celsius
2. Mid-load
   - Dry: Approx. 100 degrees Celsius
   - Poor lubrication: Approx. 60 degrees Celsius
   - Continuous lubrication: Approx. 50 degrees Celsius
3. Low load
   - Dry: Approx. 90 degrees Celsius
   - Poor lubrication: Approx. 55 degrees Celsius
   - Continuous lubrication: Approx. 50 degrees Celsius

3.1.1 High-Load

3.1.1.1 Full-lubricated

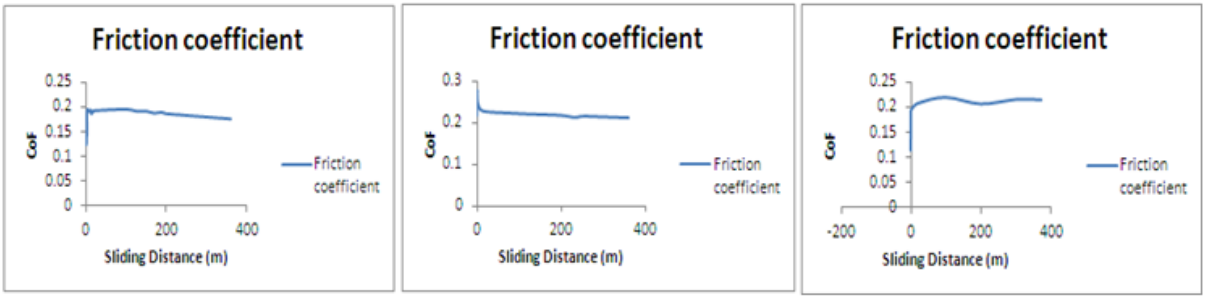

a) S1 b) S2 c) S3

Fig.1.The friction coefficient (Vertical) Vs sliding distance in meters (Horizontal) with 500N normal load and Full-Lubricated.

By applying 500N load and constantly exposing the surface with oil, the coefficient of friction in test steels behave in different ways as are illustrated above.

Fig1 shows that CoF in S1 starts from 0.13, sharply rises up to 0.2 in a very short sliding distance and with a very mild trend falls slightly and ends up at about 0.18 after sliding distance of 400m.

S2 then shows a very different trend at the beginning by starting with a CoF value of about 0.21 and a sharp rise up to 0.28 followed by a sudden fall down to 0.23 which all happens in a short time with a very short sliding distance, but then this continues by a gradual decrease and end at about 0.2 after sliding distance of 400 units.

Last material S3 at the beginning of sliding indicates a CoF of about 0.11 and rises up to 0.2 very fast and then at this point moderates the trend but still grows up to 0.22 after 100m of sliding distance. Here at this point CoF falls with a similar slope back to 0.2 after another 100m of sliding distance, and repeats a similar trend with up and down again up to 400m of sliding distance.

3.1.1.2 Dry

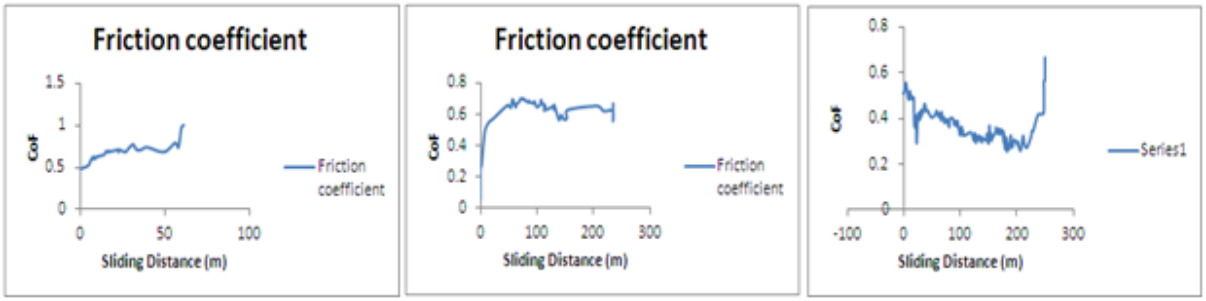

a) S1 b) S2 c) S3

Fig.2.The friction coefficient (Vertical) Vs sliding distance in meters (Horizontal) with 500N normal load, Dry.

In dry condition S1demonstrates a gradual uprising trend with irregularities and several up and downs in CoF during the test period but then after about 60m of sliding distance we observe a drastic rise in CoF up to 1 and that is the point we finish the test.

S2 starts with a CoF of 0.08 followed by a sharp rise up to 0.5 after a few sliding units. This turns to a rise with a moderate slope but including several irregular changes and reaches up to 0.7 after about 75m sliding and her eat this point we observe a gradual fall in trend which lasts until 150 sliding units and it ends up at about 0.5 where it rises again moderately and when it gets up to 0.6 at about 250m of sliding distance it indicates a sharp rise which means to stop the test.

S3 starts with CoF of 0.5 and follows down to 0.25 at about 200m of sliding distance. During this period material indicates drastic changes in CoF in very short times and they appear as peaks up and down on the chart. The lowest peak shows CoF of about 0.3 and it occurs after 30m sliding. This material changes the behavior after about 250m of sliding distance and climbs straight up and test ends.

3.1.1.3 Poor-Lubricated

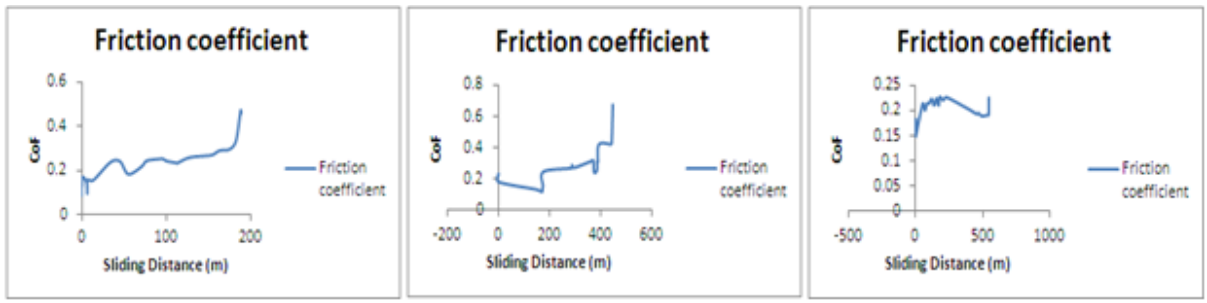

a) S1 b) S2 c) S3

Fig.3.The friction coefficient (Vertical) Vs sliding distance in meters (Horizontal) with 500N normal load with Poor-Lubricated.

S1 illustrates a growing trend in poor lubrication condition. It starts with a CoF of 0.1, jumps up to 0.18 immediately and follows up to 0.28 and then suddenly shows a drastic rise after about 170m of sliding distance. The diagram indicates namely a gradual rise during the test period but still some sharp changes are observed.

S2 starts with CoF of 0.23 and starts decreasing this value with a very small slope. With some irregularities in friction changes during the test period it ends up at 0.2 after about 550m of sliding distance.

Finally S3 comes with CoF of 0.18 falls down to 0.15 in a very short time but again rises up to 0.21 with a partially sharp slope and then follows up with a more moderate trend but with some sharp up and downs until CoF gets up to 0.23 at about 200m sliding distance and there falls till it gets to CoF of 0.18 at 500 sliding distance units. Between 500m and 600m we do not see any considerable change but after 600m CoF value flies straight up.

3.1.2 Mid-load

3.1.2.1 Full-lubricated

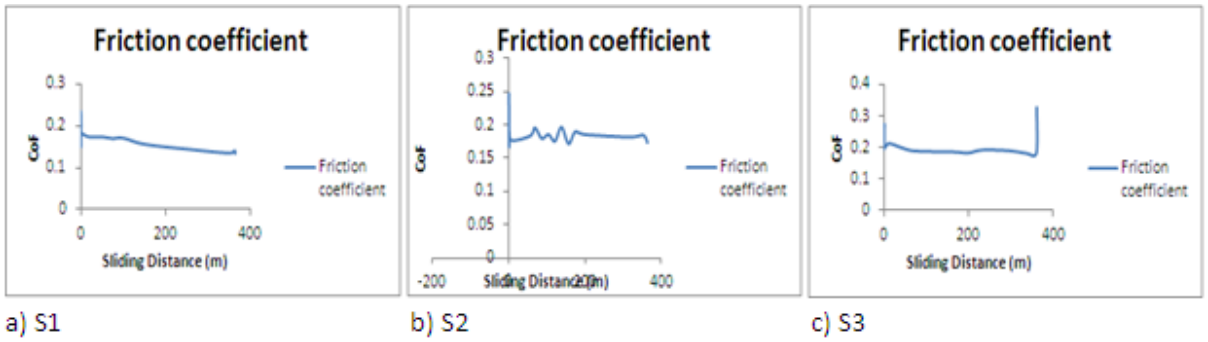

Fig.4.The friction coefficient (Vertical) Vs sliding distance in meters (Horizontal) with 370N normal load and Full-Lubricated.

In this figure we can see that S1 has a negative slope which means the CoF is decreasing by the time such as it starts with about 0.18 and ends up at 0.14 after 360 units of sliding distance.

S2 on the other hand does not show much change in CoF during the test period. We observe some small changes but overall trend shows a very close range from the start to the end.

S3 also shows very small changes in CoF, it starts at about 0.2 and ends up at 0.18 after over 350m sliding. But here at this point we observe a rise straight up in the CoF value.

3.1.2.2 Dry

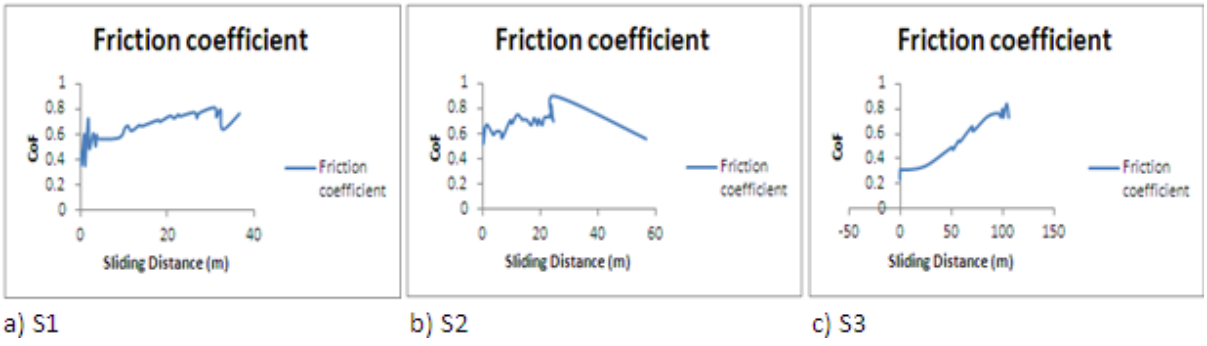

Fig.5.The friction coefficient (Vertical) Vs sliding distance in meters (Horizontal) with 370N normal load, Dry.

Mid-Load and dry condition causes the all three samples to show unstable friction behavior. S1 starts from 0.4, with several sudden shifts, it rises up to 0.8 after 30m sliding. Then at this point we see CoF falls to 0.55 sharply and again starts rising up.

S2 but is initiated with CoF of 0.6 and with all the irregular shifts it has a moderate rising trend which leads the CoF to 0.75 after 35m sliding. Here at this point we observe a sharp jump up to 0.9.

S3 starts with 0.3 and rises all the way up to 0.9 in the course 100m sliding, and then continues rising with a sharp slope.

3.1.2.3 Poor-lubricated

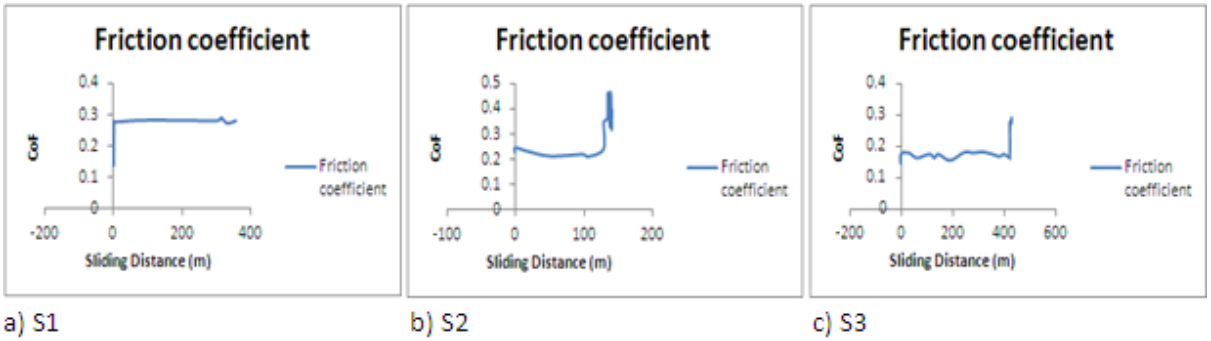

Fig.6.The friction coefficient (Vertical) Vs sliding distance in meters (Horizontal) with 370N normal load and Poor-Lubricated.

S1 starts below 0.15 and jumps right up to 0.28 then from this point to the end of the test stage which is about 400m of sliding distance, it keeps the CoF at the same range and we do not see considerable changes in it.

S2 but starts at about 0.25 then decreases the CoF very gradually till it gets to 0.2 after about 130m sliding but then at this point it sharply rises up to 0.45 and it is just 150m sliding.

S3 shows a slightly different trend. It starts with a CoF of 0.5 and falls with a slope which is bigger than the one in S2, but during this test we observe several irregular changes in CoF until it gets to 0.25 after about 220m sliding but at this point it shows a drastic rise in CoF which ends up at 0.7 at 250m sliding.

3.1.3 Low-load

3.1.3.1Full-lubricated

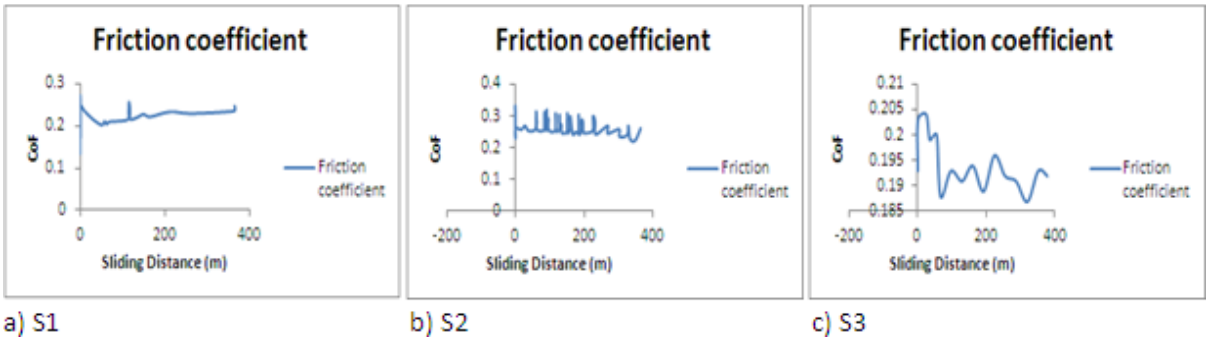

Fig.7.The friction coefficient (Vertical) Vs sliding distance in meters (Horizontal) with 270N normal load and Full-Lubricated.

S1 initiates the CoF at 0.25 and indicates a decrease in this value down to 0.2 after just 50m of sliding distance and then again rises with a very gradual slope and continues the same trend up to 0.24 after about 380m.

S2 on the other hand indicates a trend with many irregular changes such as sharp but short term rises in CoF value. This trend starts at 0.25 and ends up at almost the same value for CoF.

S3 but shows a very different trend from two others. It starts with CoF of 0.153 and rises up to 0.204 immediately in a short time and sliding distance. Here at this point we observe a fall in the CoF value; it goes down to 0.188 in the course of 50m of sliding distance. Then it slightly grows back to 0.154, again down to 0.188 and this trend repeats to the end of the test process which is about 400m sliding. Overall review of the trend gives a negative slope for the CoF value.

3.1.3.2 Dry

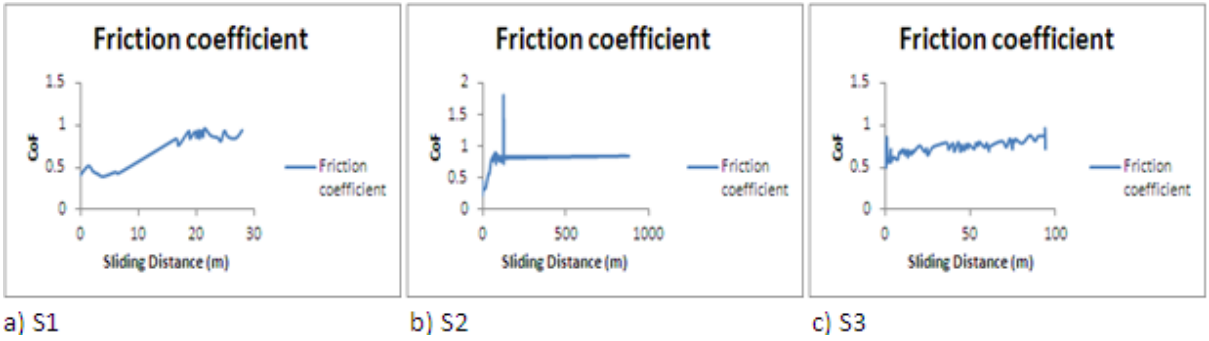

Fig.8.The friction coefficient (Vertical) Vs sliding distance in meters (Horizontal) with 270N normal load, Dry.

S1 here initiates a CoF of 0.4 and rises slightly up to 0.5 with gradual slope. At this point we observe that CoF falls down below 0.4 with the same slope and rises up again and follows to 0.8 at about 15m sliding. Then after this we do not see considerable and stable changes in CoF value until about 50m sliding, but then it rises sharp up.

S2 starts with CoF of 0.2 and begins to rise fast so that it gets up to 0.8 after about 100m sliding. After this point the material does not show any considerable change and it more or less remains stable around 0.8 and this continues until the end of test period which is about 900m sliding.

S3 shows a stable up rising trend from the beginning and follows it during most of the test period including irregularities; just at the very last moment of the test period which is around 100m sliding it indicates a drastic increase in CoF.

3.1.3.3 Poor-Lubricated

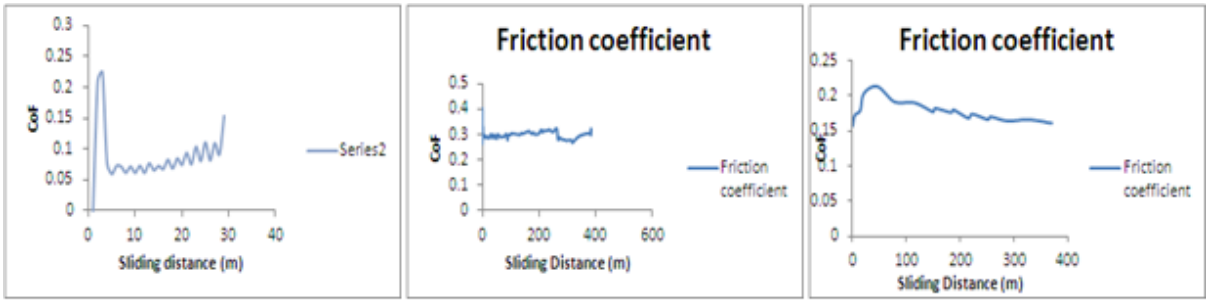

a) S1 b) S2 c) S3

Fig.9.The friction coefficient (Vertical) Vs sliding distance in meters (Horizontal) with 270N normal load, Poor-Lubricated.

As can be seen in the diagrams; S1 initially indicates a very small CoF but rises up sharply to 0.22 after a very small sliding distance, but again falls down to 0.07 with a very similar slop as it rose up. From this point CoF rises gradually up to 0.1 after over 28m sliding and then suddenly rises straight up.

S2 does not show serious changes in CoF from the start up till 400m sliding. We can just see small up and downs during the test period but after all it shows a general trend of horizontal line for CoF.

S3 starts with a CoF of 0.16 and rises up to 0.22 after about 30m sliding but then it starts decreasing the friction gradually with such a trend that after 400m we can see CoF is around the value it started with.

4. Wear

4.1 Worn areas

After finishing the tests, by checking the samples surfaces we could see that the wider the contact area was the more material has been removed from the surface.

Regarding this fact, and since we will just compare the results of the tests for these three materials, we will not calculate the actual amount of the removed material on each sample block and compare the area of contact on the samples.

4.1.1 High-Load

4.1.1.1 Full-Lubricated

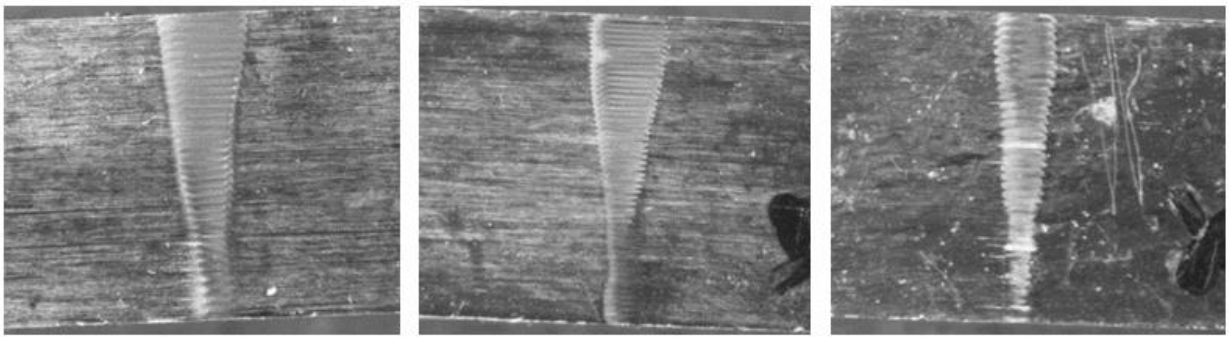

a) S1 b) S2 c) S3

Fig.10: contact area of the blocks in the tests with 500N load and Full-Lubricated

The contact areas of the samples above are as follows;

S1: $2.300 \times 10 = 23\ mm^2$

S2: $2.120 \times 10 = 21.2\ mm^2$

S3: $1.992 \times 10 = 19.92\ mm^2$

4.1.1.2 Dry

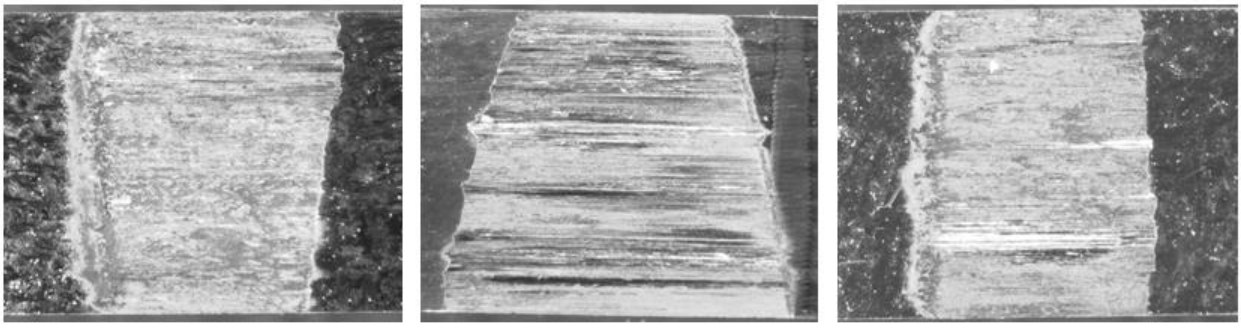

a) S1 b) S2 c) S3

Fig.11: contact area of the blocks in the tests with 500N load and Dry

Contact areas;

S1: $4.239 \times 10 = 42.39\ mm^2$

S2: $4.625 \times 10 = 46.25\ mm^2$

S3: $4.141 \times 10 = 41.41\ mm^2$

4.1.1.3 Poor-Lubricated

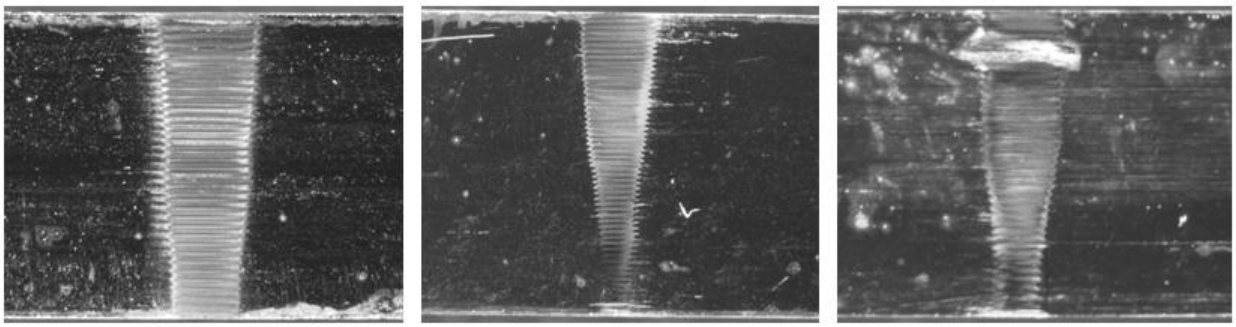

a) S1 b) S2 c) S3

Fig.12: contact area of the blocks in the tests with 500N load and Poor-Lubricated

Contact areas;

S1: $2.545 \times 10 = 25.45\ mm^2$

S2: $1.828 \times 10 = 18.28\ mm^2$

S3: $2.236 \times 10 = 22.36\ mm^2$

4.1.2 Mid-Load

4.1.2.1 Full-lubricated

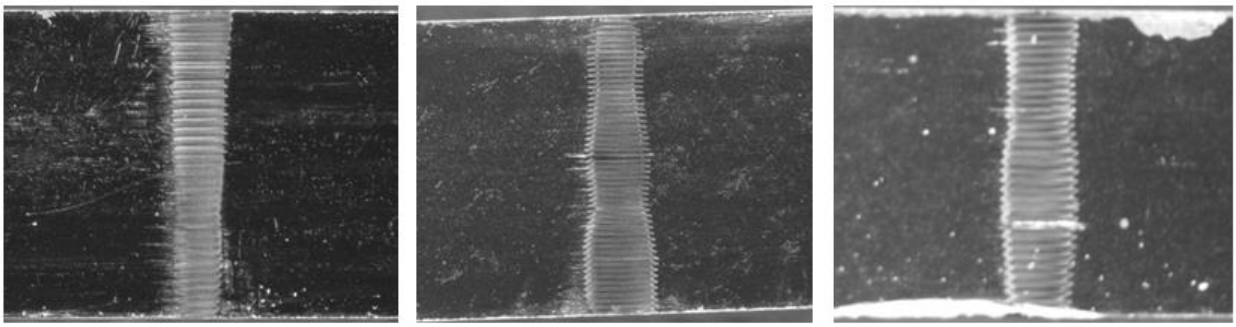

a) S1 b) S2 c) S3

Fig.13: contact area of the blocks in the tests with 370N load and Full-Lubricated

Contact areas;

S1: $2.172 \times 10 = 21.72\ mm^2$

S2: $2.298 \times 10 = 22.98\ mm^2$

S3: $2.364 \times 10 = 23.64\ mm^2$

4.1.2.2 Dry

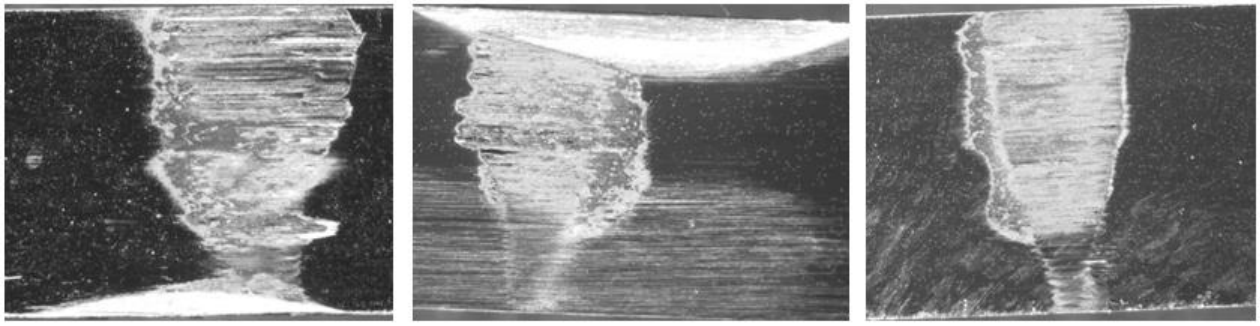

a) S1 b) S2 c) S3

Fig.14: contact area of the blocks in the tests with 370N load and Dry

Contact areas;

S1: $3.149 \times 10 = 31.49\ mm^2$

S2: $2.798 \times 10 = 27.98\ mm^2$

S3: $2.700 \times 10 = 27\ mm^2$

4.1.2.3 Poor-Lubricated

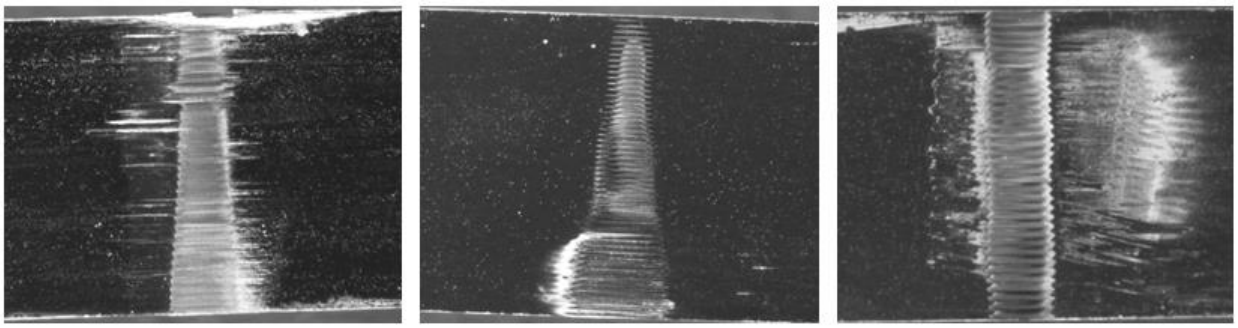

a) S1 b) S2 c) S3

Fig.15: contact area of the blocks in the tests with 370N load and Poor-Lubricated

Contact areas;

S1: $2.210 \times 10 = 22.1\ mm^2$

S2: $2.346 \times 10 = 23.46\ mm^2$

S3: $2.004 \times 10 = 20.04\ mm^2$

4.1.3 Low-Load

4.1.3.1 Full-Lubricated

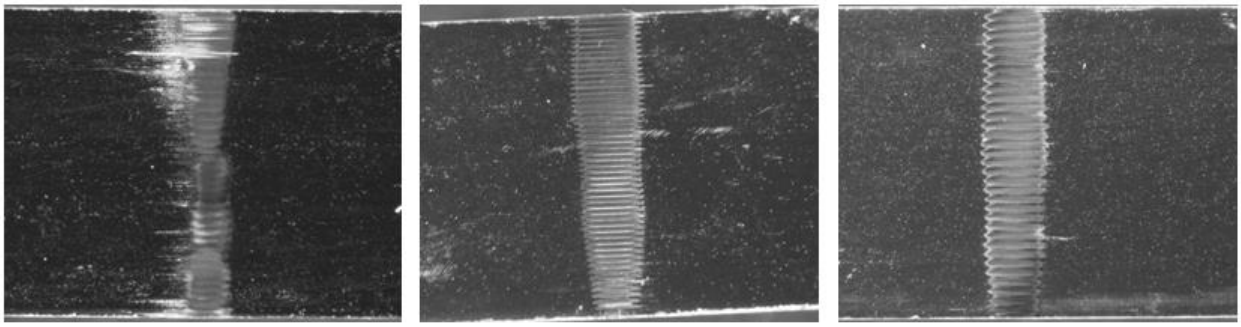

a) S1 b) S2 c) S3

Fig.16: contact area of the blocks in the tests with 270N load and Full-Lubricated

Contact areas;

S1: $2.105 \times 10 = 21.05\ mm^2$

S2: $2.223 \times 10 = 22.23\ mm^2$

S3: $2.204 \times 10 = 22.04\ mm^2$

4.1.3.2 Dry

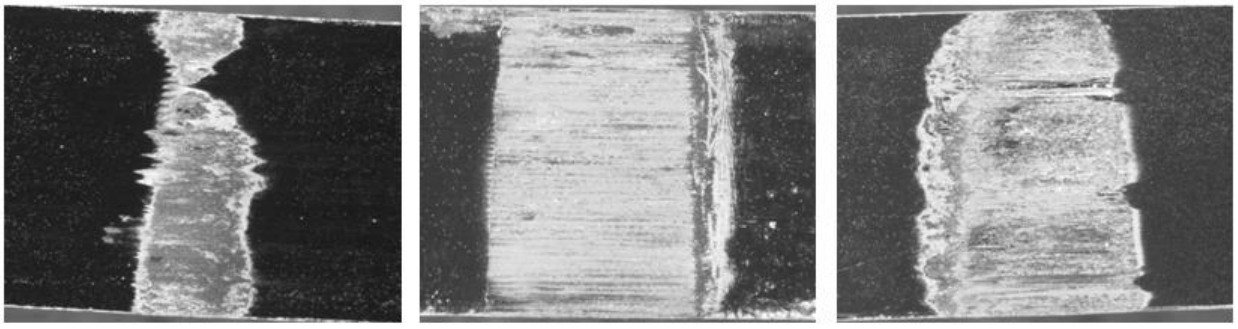

a) S1 b) S2 c) S3

Fig.17: contact area of the blocks in the tests with 270N load and Dry

Contact areas;

S1: $2.333 \times 10 = 23.33\ mm^2$

S2: $4.144 \times 10 = 41.44\ mm^2$

S3: $3.563 \times 10 = 35.63\ mm^2$

4.1.3.3 Poor-Lubricated

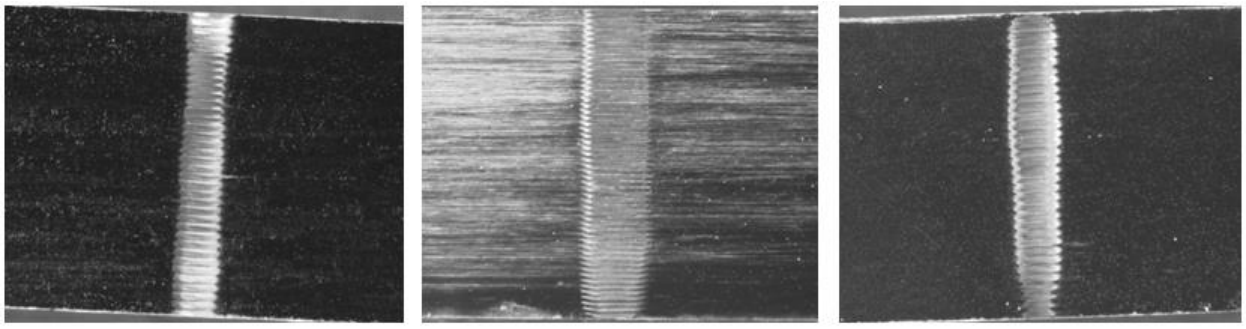

a) S1 b) S2 c) S3

Fig.18: contact area of the blocks in the tests with 270N load and Poor-lubricated

Contact areas;

S1: $2.088 \times 10 = 20.88\ mm^2$

S2: $2.957 \times 10 = 29.57 mm^2$

S3: $1.700 \times 10 = 17\ mm^2$

4.2 Wear rates

Here can see the wear rates of each material in different conditions put together on a diagram. On these diagrams the vertical axis indicates the applied load and the horizontal axis is the worn area.

As can be seen on the diagrams the blue dots represent the Full-Lubricated condition, the red dots represent the Poor-Lubricated condition and finally the green dots represent the Dry or Dry condition.

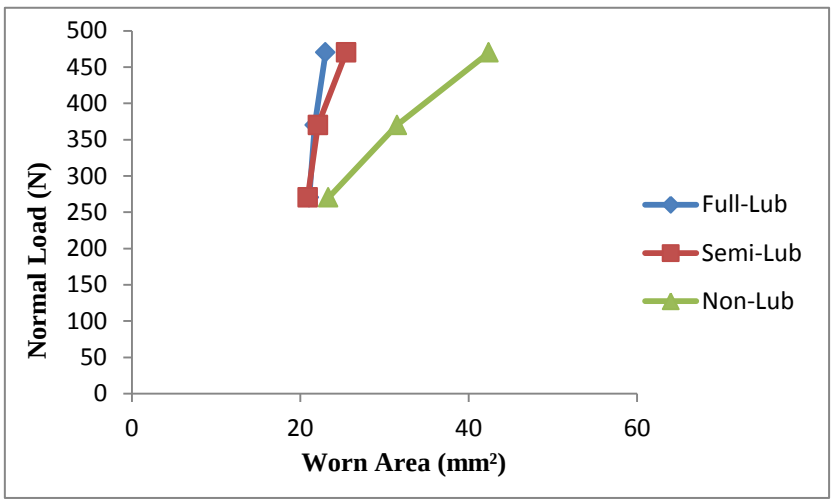

Fig.19: S1 wear rates

Regarding Fig.19, at low load the wear rate of the Full-Lubricated sample (21.05 mm^2) is slightly above the wear rate on Poor-Lubricated one (20.88 mm^2), and this is while the wear rate of the Dry sample stands above all (23.33 mm^2).

For the same material at Mid-Load condition, the Full-Lubricated sample ends up with a worn area of 21.72 mm^2 . The Poor-Lubricated block gives 22.1 which is still close to the Full-Lubricated sample.

However the Dry sample with 31.49 mm^2 worn area, indicates a considerable difference with the Low-Load wear rate, this material in High-Load condition gives 23 mm^2 worn area for Full-Lubricated, 25.45 mm^2 for Poor-Lubricated and 42.39 mm^2 for Dry samples.

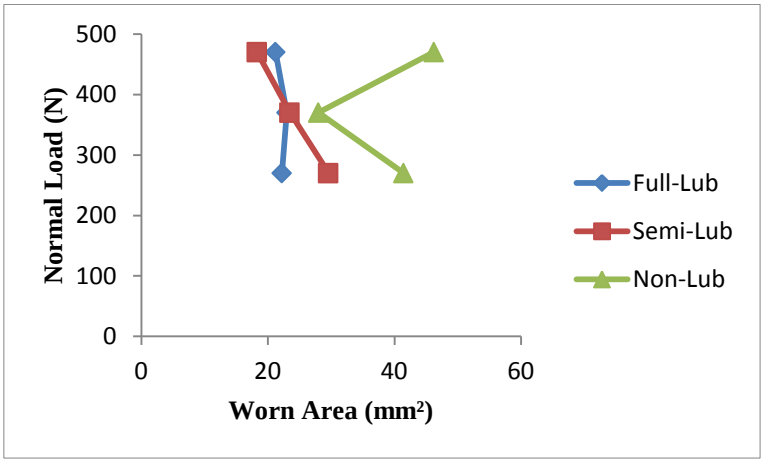

Fig.20: S2 wear rates

Fig.20 indicates the wear rate of the S2 in three different conditions.

With low-load the S2 material gets a worn area of 22.23 mm^2, 29.57 mm^2 and 41.44 mm^2 for Full-Lubricated, Poor-Lubricated and Dry conditions respectively.

With Mid-Load these values shift to 22.98 mm^2, 25.46 mm^2 and 27.98 mm^2 with same respect.

And finally these values turn to 21.2 mm^2, 18.28 mm^2 and 46.25 mm^2 for High-Load with the same respect.

Here for this material we are observing higher wear rates are registered for Low-Load tests. And relatively lower rates for Mid-Load tests, which are more obvious on Dry and Poor-Lubricated samples.

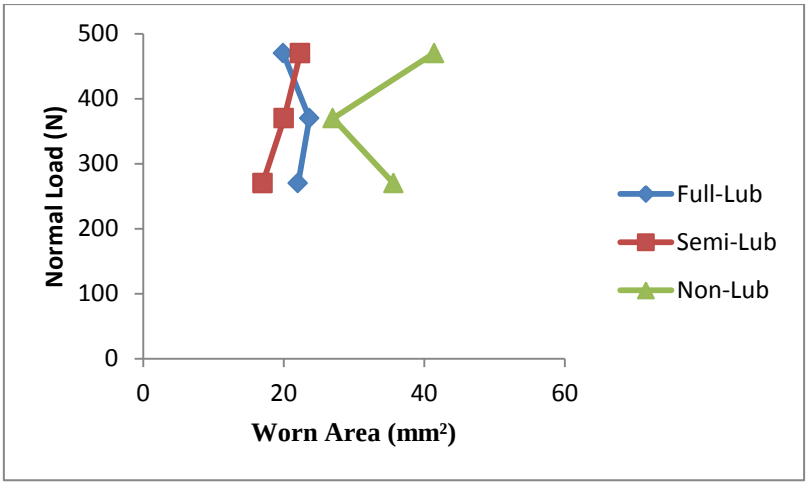

Fig.21: S3 wear rates

Fig.21 indicates the wear rate of the S3 in three different conditions. With Low-Load worn areas are registered as 22.04 mm², 17 mm² and 35.63 mm² for Full-Lubricated, Poor-lubricated and Dry conditions respectively. With mid-load these values shift to 23.64 mm², 20.04 mm² and 27 mm² with same respect. And finally these values turn to 19.92 mm², 22.36 mm² and 41.41 mm² for High-Load with the same respect.

5. Contact surface morphology and chemical compositions

5.1 S1

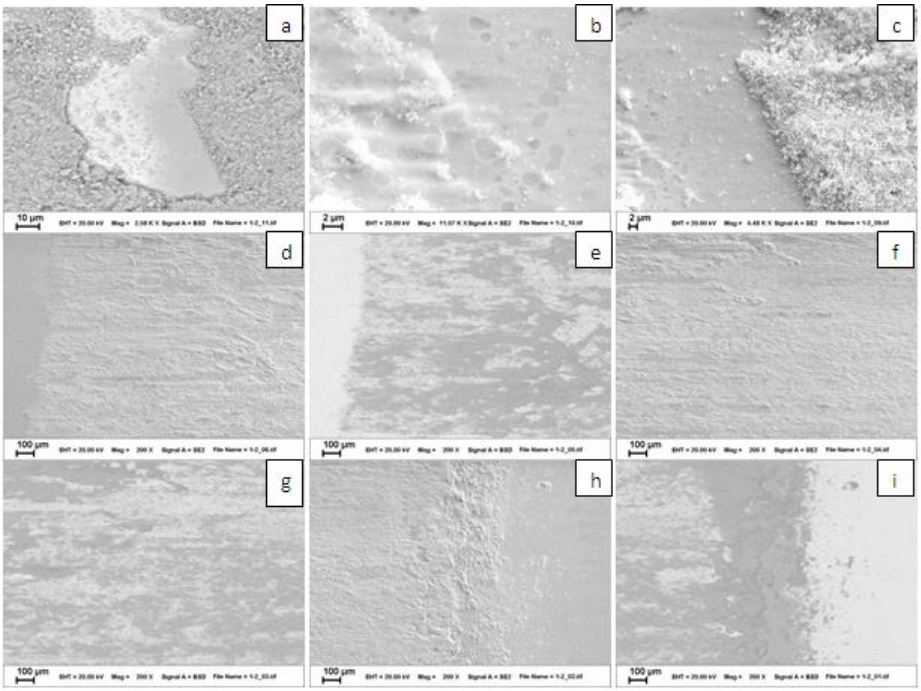

Fig.22: Morphology of S1, High-Load, Dry obtained by SEM

Fig.22 shows the worn surface of an S1 sample of the Dry, High-Load test. In Fig.22-a, b and c we can see loose particles within the tribo-layer of the contact surface which later with EDX analysis we will see that these are the oxide films formed on the surface. Fig.22-d and e illustrate the start point of the contact surface regarding the rotational direction of the cylinder. Fig.22-f and g showing the further to the middle of the contact area, and Fig.22-h and i show the end point of the contact surface where the removed material (tribo-layers) from all over the contact surface is collected there so that we see a thick dark layer all the way through this line. Later in EDX analysis results of some points on this region we will see that this layer include rich oxides.

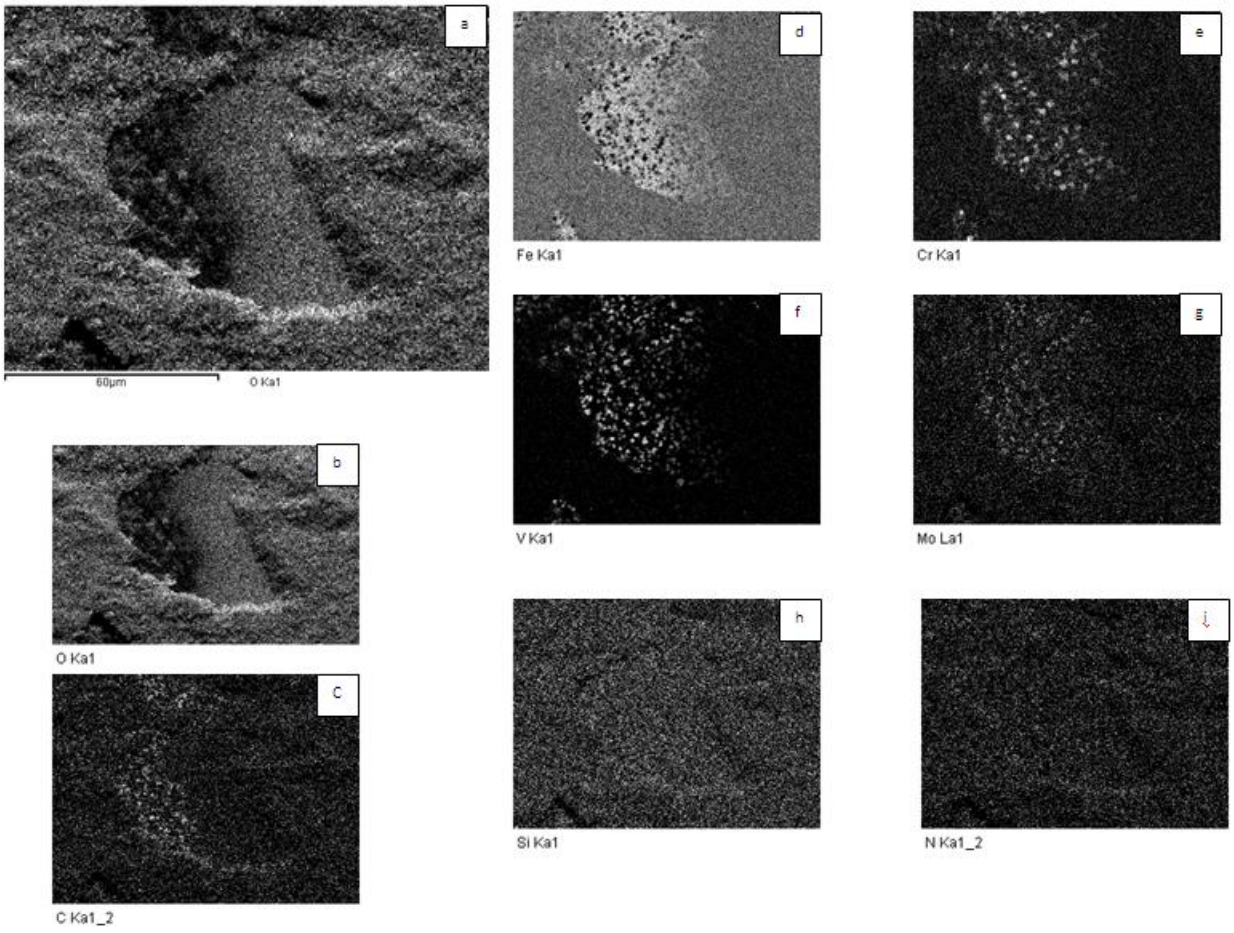

Fig.23: SEM image and X-ray elemental mapping of S1, showing the alloying elements distribution on the surface. Taken from the area which is shown in Fig.22 a, b and c.

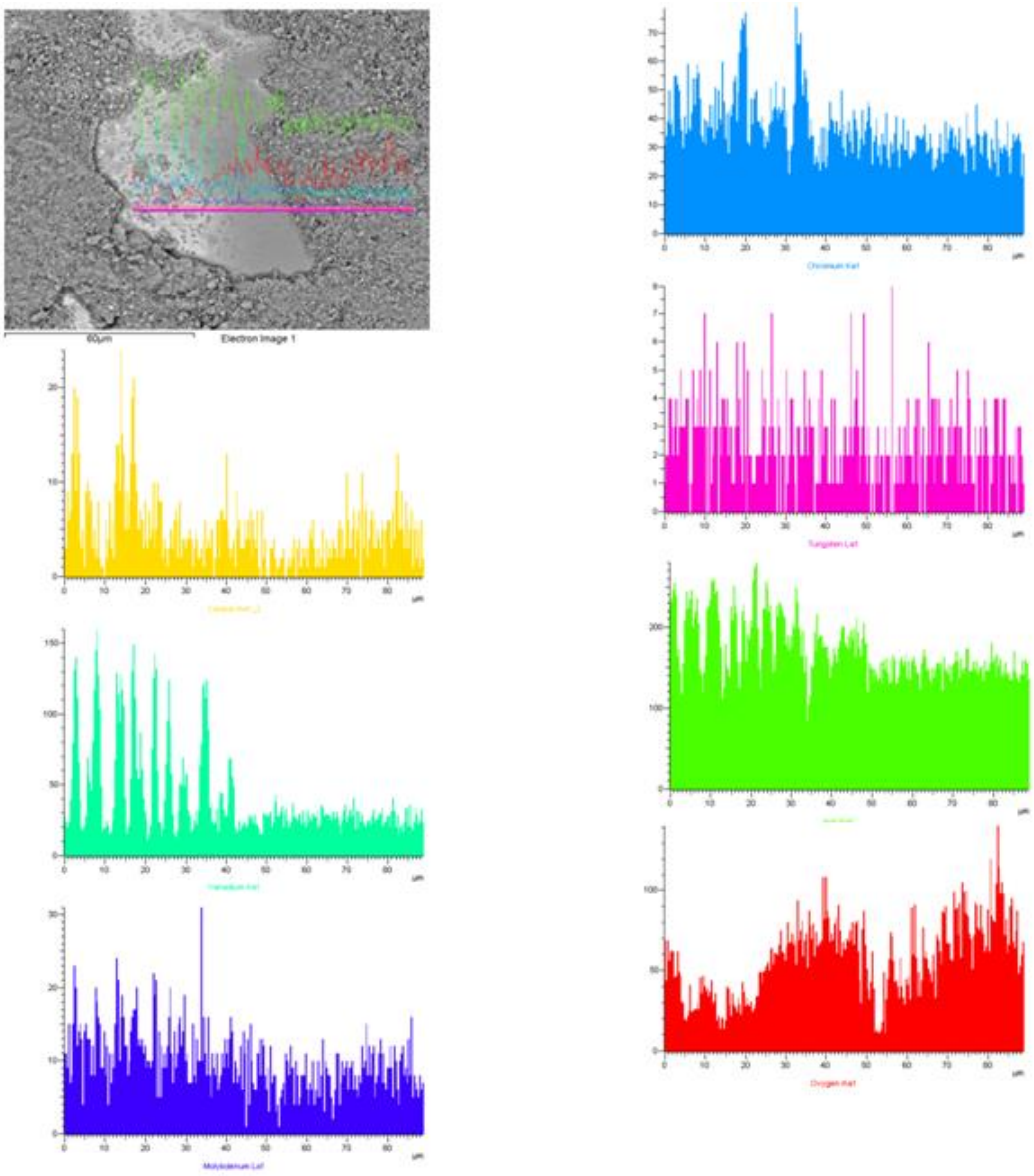

Fig.24: SEM image and X-ray elemental mapping of S1, showing the alloying elements distribution over the surface of the area shown in Fig.23.

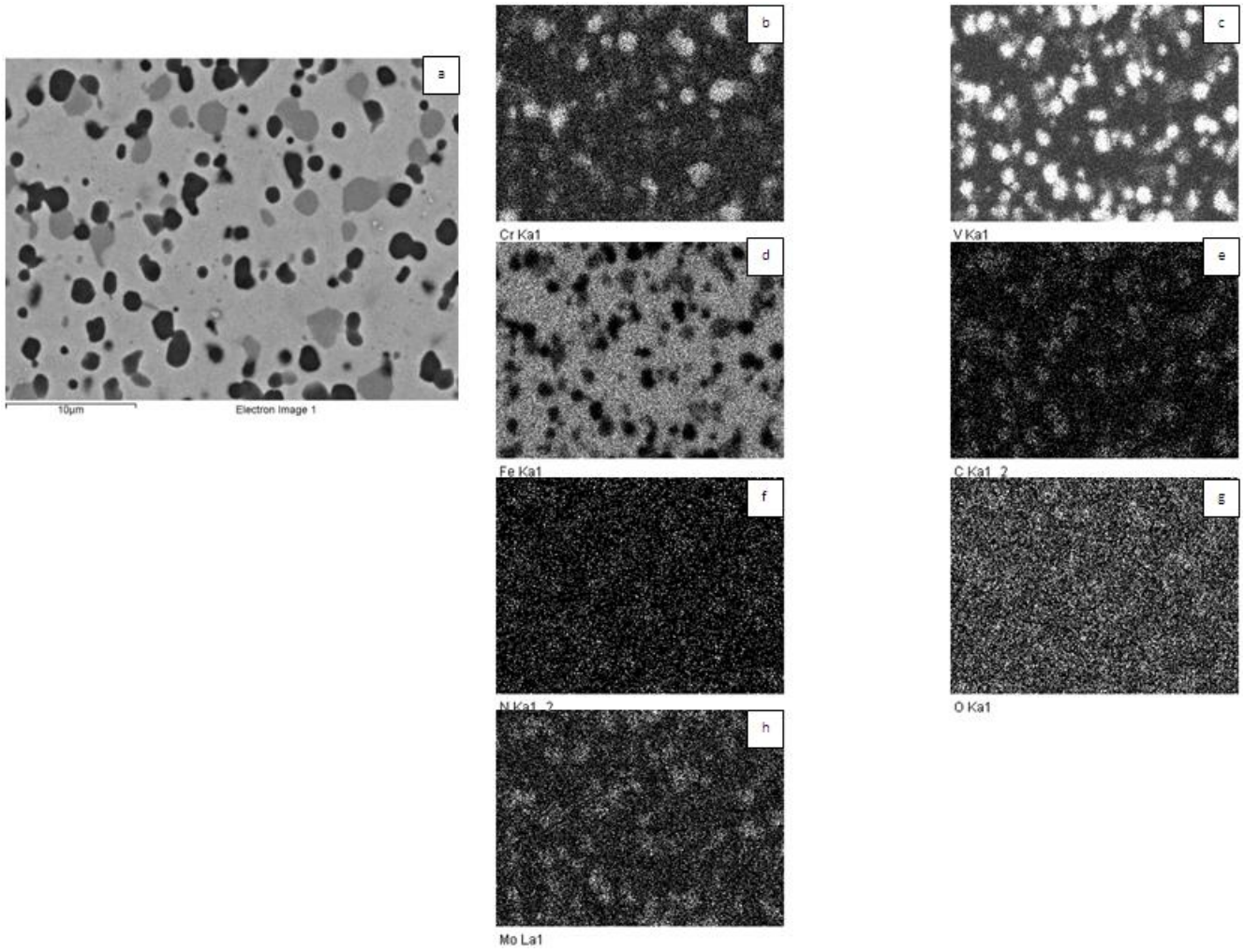

Fig.25: SEM image and X-ray elemental mapping of the bulk material of S1, showing the alloying elements distribution on the surface before the test.

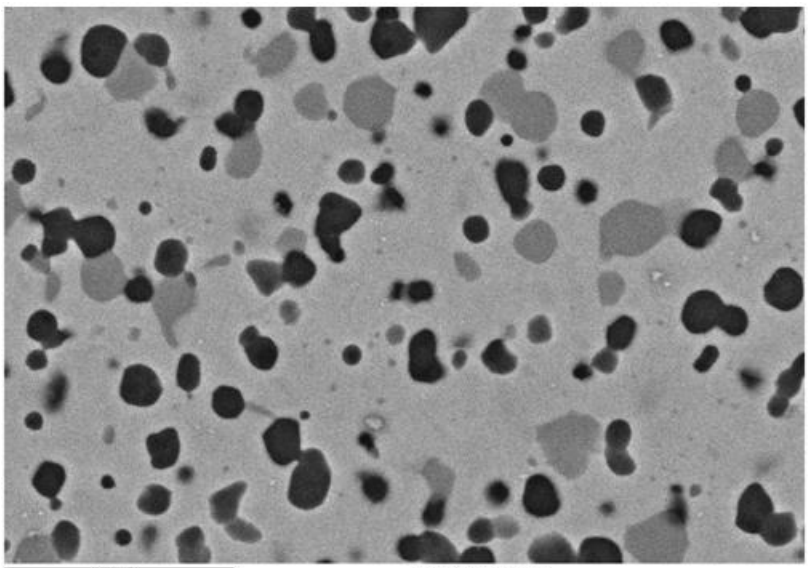

Processing option : All elements analysed

Spectrum	In stats.	C	O	Si	V	Cr	Fe	Mo
Sum Spectrum	Yes	27.37	5.30	0.90	8.90	6.33	50.37	0.82
Mean		27.37	5.30	0.90	8.90	6.33	50.37	0.82
Std. deviation		0.00	0.00	0.00	0.00	0.00	0.00	0.00
Max.		27.37	5.30	0.90	8.90	6.33	50.37	0.82
Min.		27.37	5.30	0.90	8.90	6.33	50.37	0.82

Fig.26: SEM backscattered image of the micro structure and the chemical composition analysis of S1.

The microstructure of the material S1 was characterized by means of scanning electron microscopy (SEM) combined with energy dispersive spectroscopy (EDS) and backscattered electron imaging, see Fig.26.

The dark (black) spots are representing the (V rich) MC and the bright (grey) spots are the (Cr.Fe) M7C3.

The signs of wear and tribo-layer characteristics were examined by means of SEM combined with EDS and using elemental X-ray mapping.
In order to characterize the wear mechanisms and tribo-layers the SEM and elemental X-ray mapping were carried out.
The wear track shows no micro-cracking and micro-ploughing, and no glazed surface. But a rich oxide layer is seen on the surface (Fig.27).

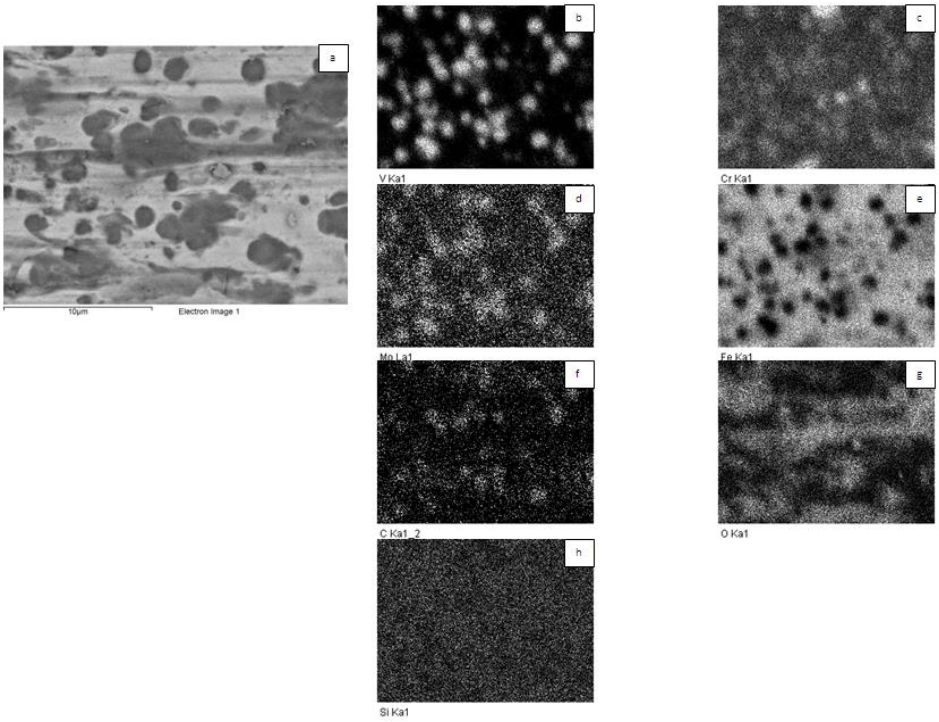

Fig.27: SEM image and X-ray elemental mapping of the wear track of S1 with High-Load, Dry condition.

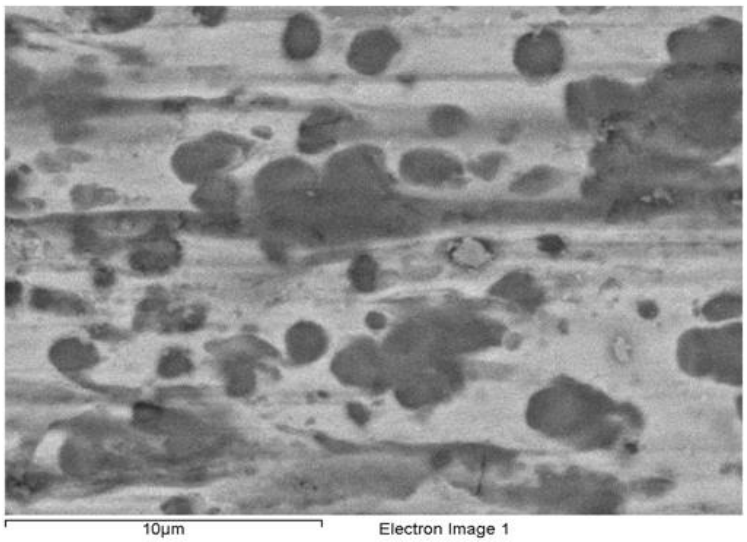

Processing option : All elements analysed

Spectrum	In stats.	C	O	Si	V	Cr	Fe	Mo
Sum Spectrum	Yes	19.19	31.08	0.62	8.37	4.38	35.66	0.70
Mean		19.19	31.08	0.62	8.37	4.38	35.66	0.70
Std. deviation		0.00	0.00	0.00	0.00	0.00	0.00	0.00
Max.		19.19	31.08	0.62	8.37	4.38	35.66	0.70
Min.		19.19	31.08	0.62	8.37	4.38	35.66	0.70

Fig.28: SEM backscattered image of the micro structure and the chemical composition analysis of S1 with High-Load, Dry condition.

Comparing Fig.26 and Fig.28 we see that the oxygen rate has increased with about 600% which indicates a high rate of oxidation on the wear track due to the temperature rise during the sliding and exposure to the air. Moreover there are signs of smearing on the surface also which has caused deformations in the particles all over the surface in the contact region.

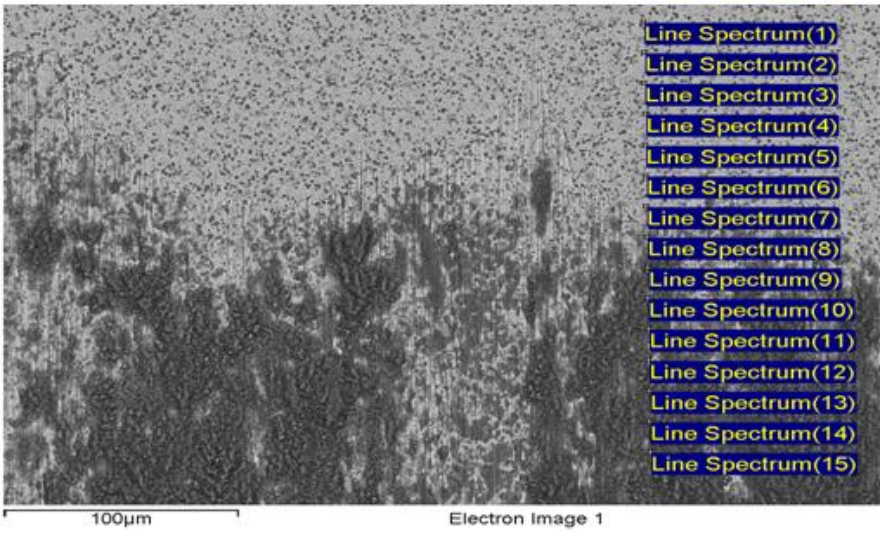

Processing option : All elements analysed

Spectrum	In stats.	C	O	Si	V	Cr	Fe	Mo
Line Spectrum(1)	Yes	17.42	3.56	1.28	1.81	4.97	70.56	0.40
Line Spectrum(2)	Yes	43.46	8.99	0.28	29.55	4.59	11.32	1.82
Line Spectrum(3)	Yes	46.90	4.67	0.44	14.98	3.96	27.87	1.18
Line Spectrum(4)	Yes	16.68	29.60	0.64	11.09	3.79	37.49	0.71
Line Spectrum(5)	Yes	16.33	5.89	1.29	4.59	5.35	66.19	0.37
Line Spectrum(6)	Yes	25.32	23.87	0.62	3.40	9.26	37.13	0.40
Line Spectrum(7)	Yes	13.62	13.26	1.23	1.43	4.88	65.23	0.35
Line Spectrum(8)	Yes	9.07	60.67	0.24	13.60	3.39	12.20	0.82
Line Spectrum(9)	Yes	10.80	52.31	0.67	3.50	2.97	29.44	0.32
Line Spectrum(10)	Yes	8.88	36.79	0.44	6.97	12.82	33.46	0.62
Line Spectrum(11)	Yes	10.47	45.25	0.52	4.79	3.76	34.82	0.40
Line Spectrum(12)	Yes	14.31	48.52	0.60	2.93	5.58	27.72	0.34
Line Spectrum(13)	Yes	12.60	55.41	0.54	2.80	3.54	24.81	0.30
Line Spectrum(14)	Yes	9.75	62.11	0.43	7.79	2.79	16.64	0.49
Line Spectrum(15)	Yes	9.94	55.13	0.50	5.75	2.67	25.61	0.41
Mean		17.70	33.74	0.65	7.67	4.96	34.70	0.59
Std. deviation		11.97	22.10	0.34	7.35	2.72	18.72	0.42
Max.		46.90	62.11	1.29	29.55	12.82	70.56	1.82
Min.		8.88	3.56	0.24	1.43	2.67	11.32	0.30

Fig.28: SEM backscattered image of the micro structure and the chemical composition analysis of 15 different line spectrums on S1 High-Load, Dry sample.

By applying line spectrum on different regions of the surface (Fig.28) we observe the change of oxygen content of the target zones.
Here we start from far outside the contact surface (bulk material) followed down to the

contact surface, from the start line side, including different areas in the contact region. The results indicating that the darker the area is the more oxygen exist.

Line spectrum (1) in the bulk zone with 3.5% oxygen content has the minimum and line spectrum (14) in the dark contact area with 62.1% oxygen content has the maximum rate of the oxygen content.

The parallel grooves on the surface caused by abrasion are most likely holding some loose oxide debris.

The picture below (Fig.29) indicates 15 different spectrums on the contact surface which are taken around the end line regarding the sliding direction. As was mentioned before at this area we observe a dark thick layer of material.
This layer contains the worn materials which have been removed from the contact surface and moved down to this area, which is right below the last contact line, collected and adhered together and built up this thick layer.
Spectrums 1 to 6 are taken from this dark thick layer and the rest of spectrums are taken from different points further inside the contact zone.

By analyzing the material and chemical composition of this thick dark layer and comparing the results with the results from other points in and outside the contact zone, we would find the main or dominant wear mechanism/s.

As we mentioned before the dark regions are high-oxide layers built up over the contact surface.
Spectrums 1 to 15 in the Figure below are all taken from the dark zones; therefore we observe almost the same range of oxygen content, including 63% oxygen at Spectrum 1 as maximum and 45% oxygen content at Spectrum 4 as minimum.

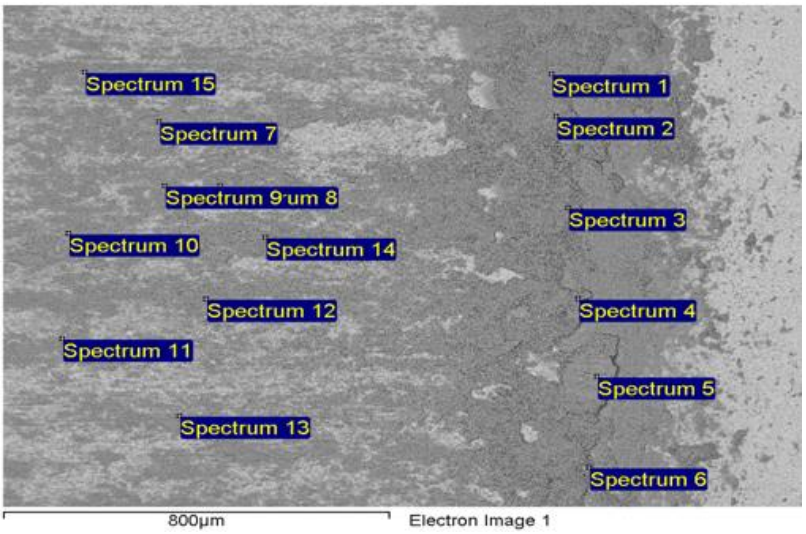

Processing option : All elements analysed

Spectrum	In stats.	C	O	Si	V	Cr	Fe	Mo
Spectrum 1	Yes	15.07	63.45	0.48	1.74	1.79	17.22	0.24
Spectrum 2	Yes	20.97	46.46	0.58	3.12	2.88	25.70	0.30
Spectrum 3	Yes	12.31	59.88	0.47	2.78	2.33	21.95	0.26
Spectrum 4	Yes	9.49	45.76	0.60	3.83	3.63	36.37	0.33
Spectrum 5	Yes	10.34	51.40	0.64	3.08	3.21	31.10	0.23
Spectrum 6	Yes	11.67	58.60	0.64	2.76	2.49	23.60	0.23
Spectrum 7	Yes	7.89	56.75	0.56	6.06	3.07	25.29	0.38
Spectrum 8	Yes	9.23	62.42	0.61	4.19	2.33	20.90	0.32
Spectrum 9	Yes	11.43	61.70	0.53	2.65	2.29	21.13	0.27
Spectrum 10	Yes	8.92	50.36	0.57	3.37	3.28	33.18	0.33
Spectrum 11	Yes	12.31	60.83	0.60	2.82	2.18	20.96	0.30
Spectrum 12	Yes	10.06	52.60	0.63	4.15	3.10	29.09	0.36
Spectrum 13	Yes	12.14	59.13	0.59	3.15	2.40	22.32	0.27
Spectrum 14	Yes	11.02	55.02	0.59	3.27	2.85	26.93	0.33
Spectrum 15	Yes	9.09	56.08	0.53	4.65	3.49	25.74	0.42
Mean		11.46	56.03	0.58	3.44	2.76	25.43	0.30
Std. deviation		3.19	5.64	0.05	1.03	0.54	5.20	0.05
Max.		20.97	63.45	0.64	6.06	3.63	36.37	0.42

Fig.29: SEM backscattered image of the micro structure and the chemical composition analysis of 15 different spectrums on S1 material surface, High-Load, Dry sample.

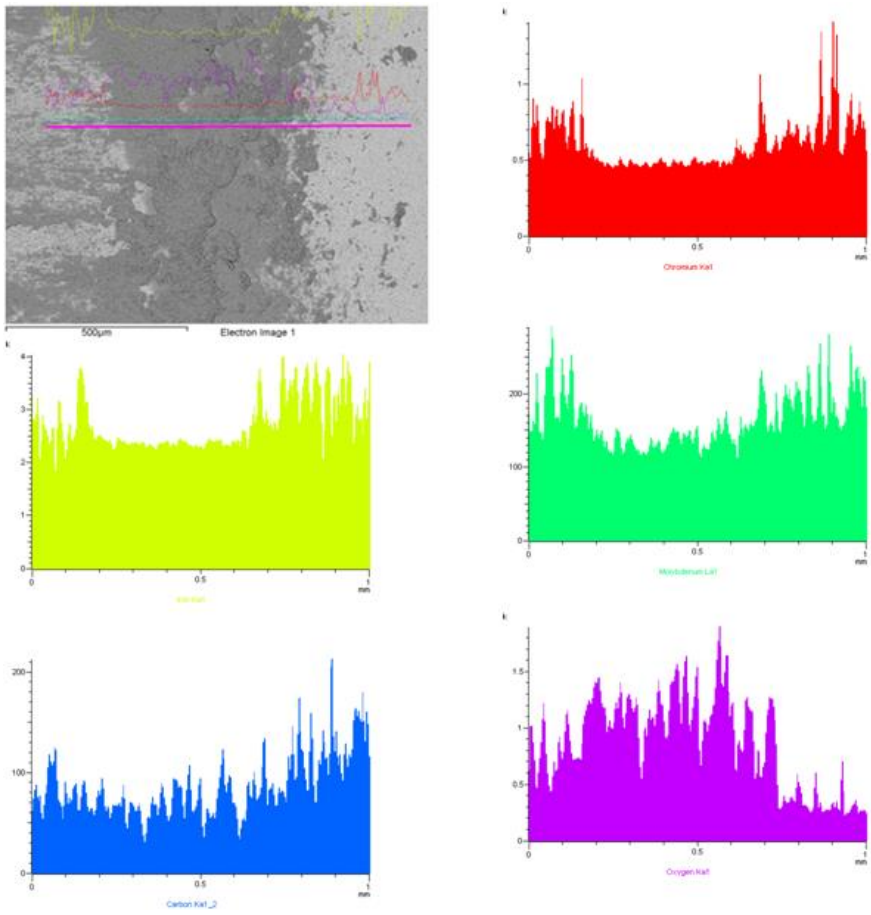

Fig.30: SEM image and X-ray elemental mapping of S1, showing the alloying elements distribution over the surface of the area shown in Fig.21.

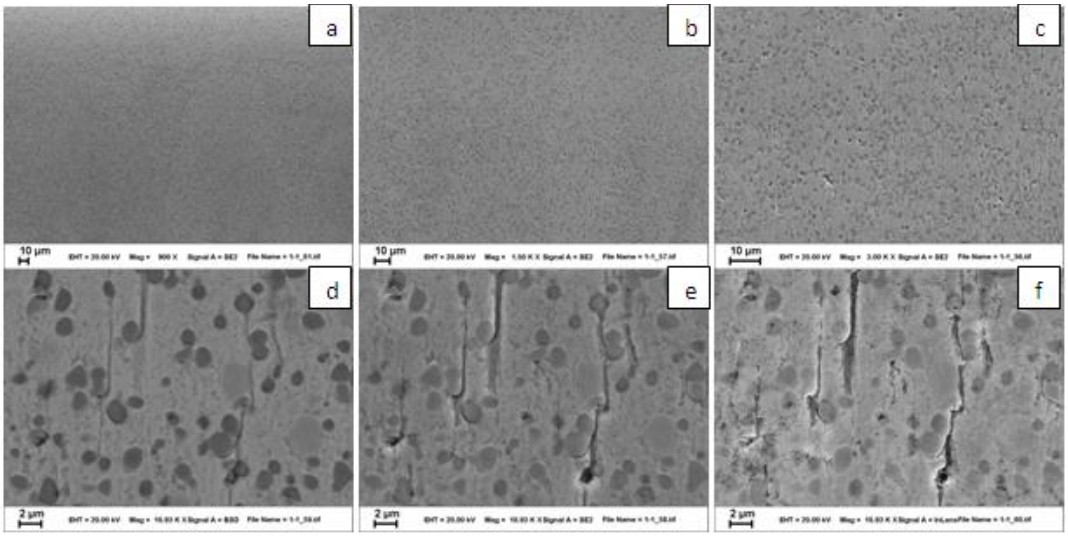

Fig.31: Morphology of S1, High-Load, Full-Lubricated obtained by SEM

Fig.31 shows the worn surface of an S1 sample of the full-lubricated, high load test. Here we do not observe loose particles or dark oxide films formed on the surface within the

contact zone, and also no smearing and no signs of abrasive wear. There are some cracks initiated within the contact area, as can be seen in Fig.31 d, e and f. Here we see that the alloying inclusions have not deformed and more or less kept their physical structures.

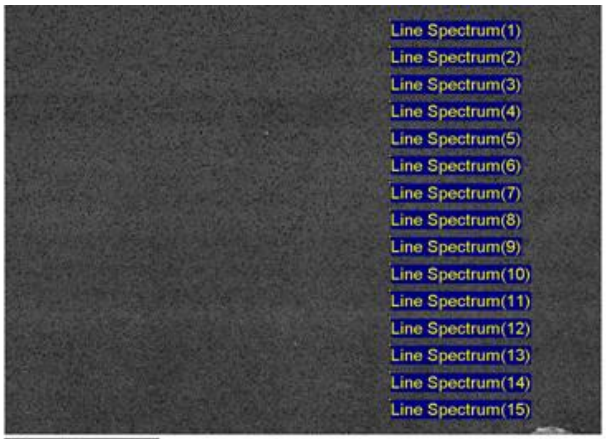

Spectrum	In stats.	C	N	O	Si	V	Cr	Fe	Mo
Line Spectrum(1)	Yes	15.11	0.64	6.68	0.91	19.40	5.78	50.36	1.12
Line Spectrum(2)	Yes	20.70	-3.99	2.48	1.16	12.56	7.71	58.26	1.12
Line Spectrum(3)	Yes	19.84	0.04	2.96	1.30	1.61	5.83	67.99	0.44
Line Spectrum(4)	Yes	23.26	-2.50	2.70	1.16	2.49	4.88	67.56	0.44
Line Spectrum(5)	Yes	16.47	-1.77	3.11	1.28	2.72	5.40	72.40	0.39
Line Spectrum(6)	Yes	16.26	-2.27	4.80	1.22	2.53	6.39	70.66	0.42
Line Spectrum(7)	Yes	25.41	0.61	8.63	0.98	3.21	4.56	56.25	0.35
Line Spectrum(8)	Yes	20.57	-1.70	20.55	0.85	4.19	4.11	50.98	0.44
Line Spectrum(9)	Yes	26.40	-4.66	11.31	0.84	6.28	8.74	50.44	0.64
Line Spectrum(10)	Yes	23.99	-2.17	15.90	0.88	3.77	4.28	52.82	0.53
Line Spectrum(11)	Yes	21.17	-1.89	26.00	0.69	6.01	4.22	43.15	0.65
Line Spectrum(12)	Yes	19.38	-0.54	13.70	1.14	1.47	4.46	59.97	0.42
Line Spectrum(13)	Yes	27.05	-2.80	16.03	0.77	4.97	4.38	49.12	0.48
Line Spectrum(14)	Yes	25.00	-3.41	13.08	1.14	2.43	4.42	56.93	0.41
Line Spectrum(15)	Yes	18.50	-2.45	26.41	0.87	2.41	5.20	48.49	0.57

Fig.32: SEM backscattered image of the micro structure and the chemical composition analysis of 15 different line spectrums on S1 High-Load, Full-Lubricated sample.

High load, full-lubricated result (Fig.32) illustrates rises in oxygen content of the contact surface up to maximum of 26% while the average oxygen content of the bulk material is around 4%. This shows that even though lubrication is of the contact surface is protective but it is not isolating the surface from oxygen exposure.

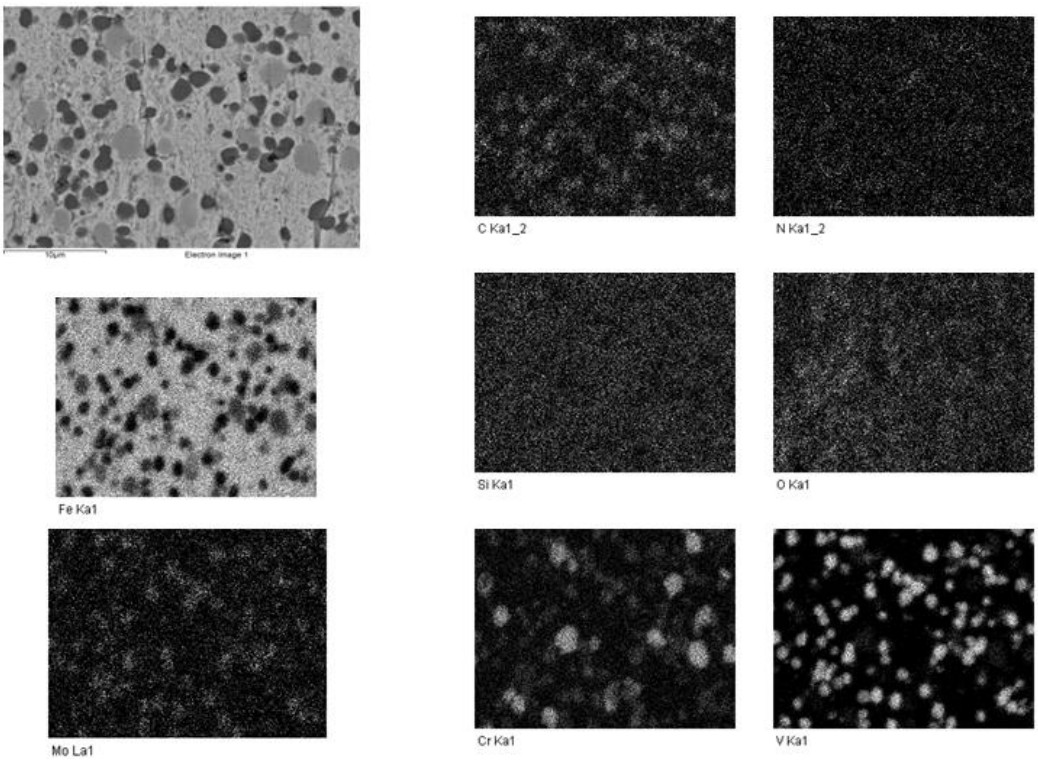

Fig.33: SEM image and X-ray elemental mapping of the wear track of S1 with High-Load, Full-Lubricated condition.

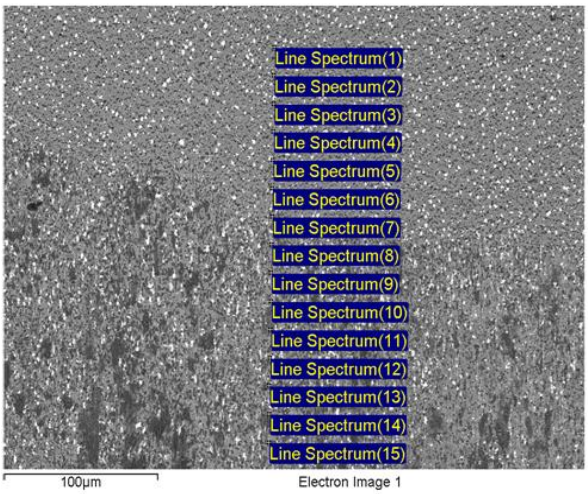

Spectrum	In stats.	C	N	O	V	Cr	Fe	Mo	W
Line Spectrum(1)	Yes	21.24	26.77	5.76	15.53	3.05	24.05	2.22	1.38
Line Spectrum(2)	Yes	19.01	-0.07	5.99	2.46	3.90	67.39	0.84	0.47
Line Spectrum(3)	Yes	18.17	3.34	6.27	3.73	3.83	63.27	0.89	0.50
Line Spectrum(4)	Yes	20.41	11.43	7.58	10.92	3.42	45.09	0.72	0.43
Line Spectrum(5)	Yes	18.36	0.73	6.82	2.59	3.89	66.33	0.79	0.49
Line Spectrum(6)	Yes	14.21	10.08	16.00	21.82	3.80	32.86	0.80	0.42
Line Spectrum(7)	Yes	18.33	4.96	8.07	3.96	3.50	59.81	0.83	0.53
Line Spectrum(8)	Yes	16.72	3.98	6.88	9.31	3.98	55.60	2.28	1.26
Line Spectrum(9)	Yes	20.57	2.65	7.21	5.55	3.43	59.26	0.87	0.45
Line Spectrum(10)	Yes	20.19	6.06	7.26	5.10	3.70	53.92	2.22	1.55
Line Spectrum(11)	Yes	18.99	0.63	36.11	2.06	2.37	38.62	0.72	0.51
Line Spectrum(12)	Yes	19.57	11.09	16.71	11.41	2.98	36.82	0.90	0.51
Line Spectrum(13)	Yes	15.42	18.13	26.74	17.27	2.60	17.87	1.26	0.69
Line Spectrum(14)	Yes	18.10	1.39	3.35	5.95	4.08	65.40	1.14	0.60
Line Spectrum(15)	Yes	20.95	15.45	10.98	13.08	2.94	34.77	1.16	0.67

Fig.34: SEM backscattered image of the micro structure and the chemical composition analysis of 15 different line spectrums on S2 High-Load, Dry sample.

Comparing the oxygen content of line spectrums (1) to (5) which are representing the bulk material surface contents (no contact with the test cylinder) with the line spectrums (6) to (15) which are taken from the contact surface, shows that the oxygen content has increased from an average of about 6% in the bulk up to about 20% over the contact surface.

But we should not neglect the fact that this test has been taken from the contact start line regarding the rotational direction.

5.2 S2

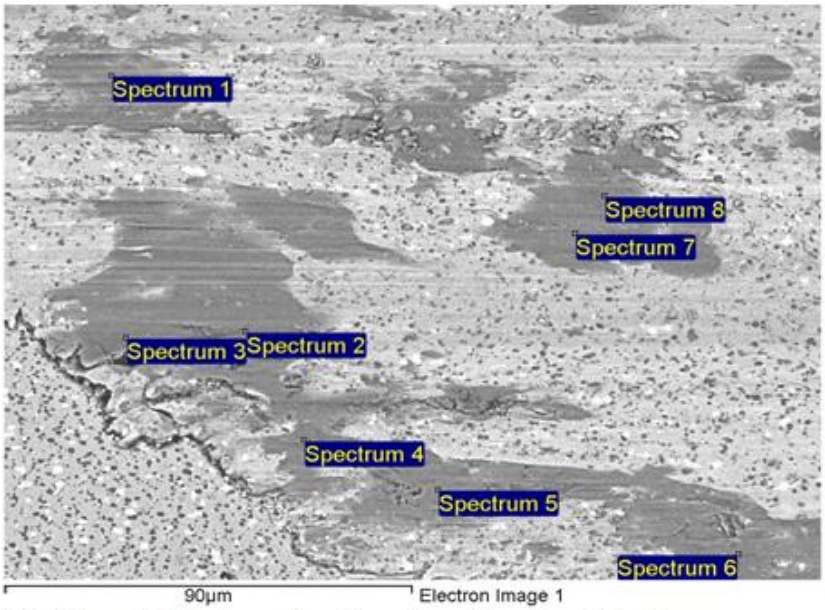

Spectrum	In stats.	C	N	O	V	Cr	Fe	Mo	W
Spectrum 1	Yes	16.14	1.22	43.59	3.56	2.18	31.84	0.90	0.57
Spectrum 2	Yes	18.76	1.17	44.26	3.92	2.20	28.25	0.77	0.66
Spectrum 3	Yes	17.68	1.21	43.89	3.81	2.53	29.34	0.94	0.60
Spectrum 4	Yes	14.58	0.90	52.52	3.70	2.04	24.82	0.83	0.61
Spectrum 5	Yes	16.13	1.18	45.33	3.87	2.33	29.50	0.94	0.73
Spectrum 6	Yes	15.01	0.28	47.64	4.16	2.13	29.13	0.98	0.67
Spectrum 7	Yes	17.05	1.02	47.00	3.50	2.16	27.79	0.86	0.61
Spectrum 8	Yes	16.72	1.28	48.20	3.71	2.31	26.33	0.87	0.58

Fig.35: SEM backscattered image of the micro structure and the chemical composition analysis of 8 different spectrums on contact surface of S2 sample of High-Load, Dry.

The electron image in the Fig.35 shows a part of contact surface of the S2 in High-Load, Dry condition. The chemical compositions of the dark regions over the surface have been examined indicating that a high rate of oxygen content has been collected within these areas. Around these areas we observe loose parts which seem to be brittle oxide layers. These parts are formed and removed layer by layer by during the sliding period.

Moreover, the long parallel grooves all over the contact surface are the effects of the abrasive wear.

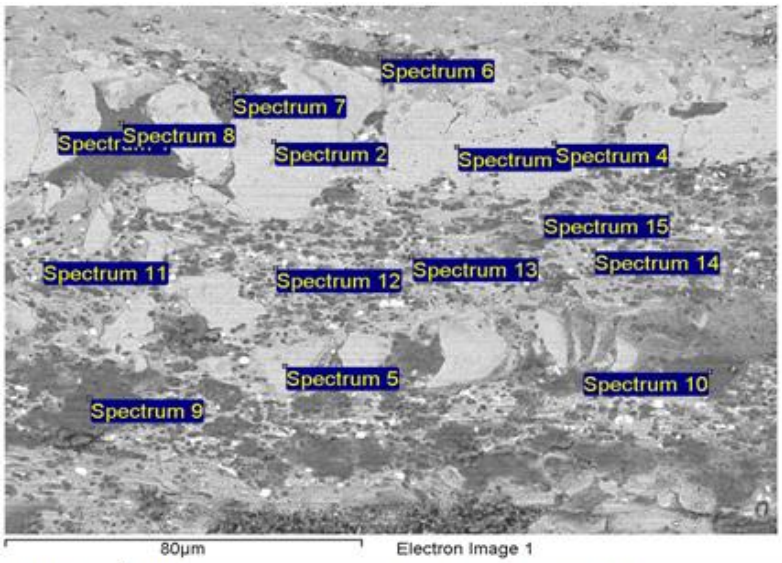

Spectrum	In stats.	C	N	O	V	Cr	Fe	Mo	W
Spectrum 1	Yes	39.38	-3.88	7.70	0.83	0.51	51.90	1.94	1.61
Spectrum 2	Yes	37.23	-4.48	7.64	0.63	0.39	54.98	2.05	1.56
Spectrum 3	Yes	40.06	-4.77	5.28	0.50	0.31	55.23	1.97	1.43
Spectrum 4	Yes	37.24	-2.32	9.15	0.70	0.51	51.32	1.85	1.57
Spectrum 5	Yes	35.53	-2.09	5.04	0.76	0.58	56.43	2.21	1.54
Spectrum 6	Yes	11.96	3.41	51.96	3.17	1.64	26.42	0.95	0.50
Spectrum 7	Yes	10.30	0.66	40.97	3.56	2.17	40.59	1.16	0.58
Spectrum 8	Yes	22.01	2.03	42.83	3.67	1.90	26.02	0.92	0.62
Spectrum 9	Yes	10.83	3.20	53.42	5.54	1.84	23.88	0.78	0.52
Spectrum 10	Yes	8.62	1.22	55.20	3.67	2.02	27.78	0.87	0.62
Spectrum 11	Yes	15.89	5.31	35.17	6.84	2.40	32.85	0.92	0.63
Spectrum 12	Yes	21.33	-0.61	16.08	2.52	2.88	55.78	1.20	0.82
Spectrum 13	Yes	11.28	1.88	39.61	3.40	2.69	39.68	0.91	0.56
Spectrum 14	Yes	18.49	21.26	20.07	15.09	2.56	21.26	0.80	0.48
Spectrum 15	Yes	23.52	-0.06	6.42	3.32	3.80	61.13	1.11	0.75

Fig.36: SEM backscattered image of the micro structure and the chemical composition analysis of 8 different spectrums on contact surface of S2 sample of High-Load, Dry.

Here (Fig.36) we chose spectrums over dark and bright regions for the chemical composition analysis to be later compare the characteristics of different areas.

As an example we compare Spectrum1 and Spectrum8, two very close points, one picked from a bright area (Spectrum1) while the other one is picked over a dark area (spectrum8).

Spectrum1 declares oxygen content of 7.7% while Spectrum8 registers it with 42.8%. This is quite obvious that the dark regions over the surface containing higher oxide rates.

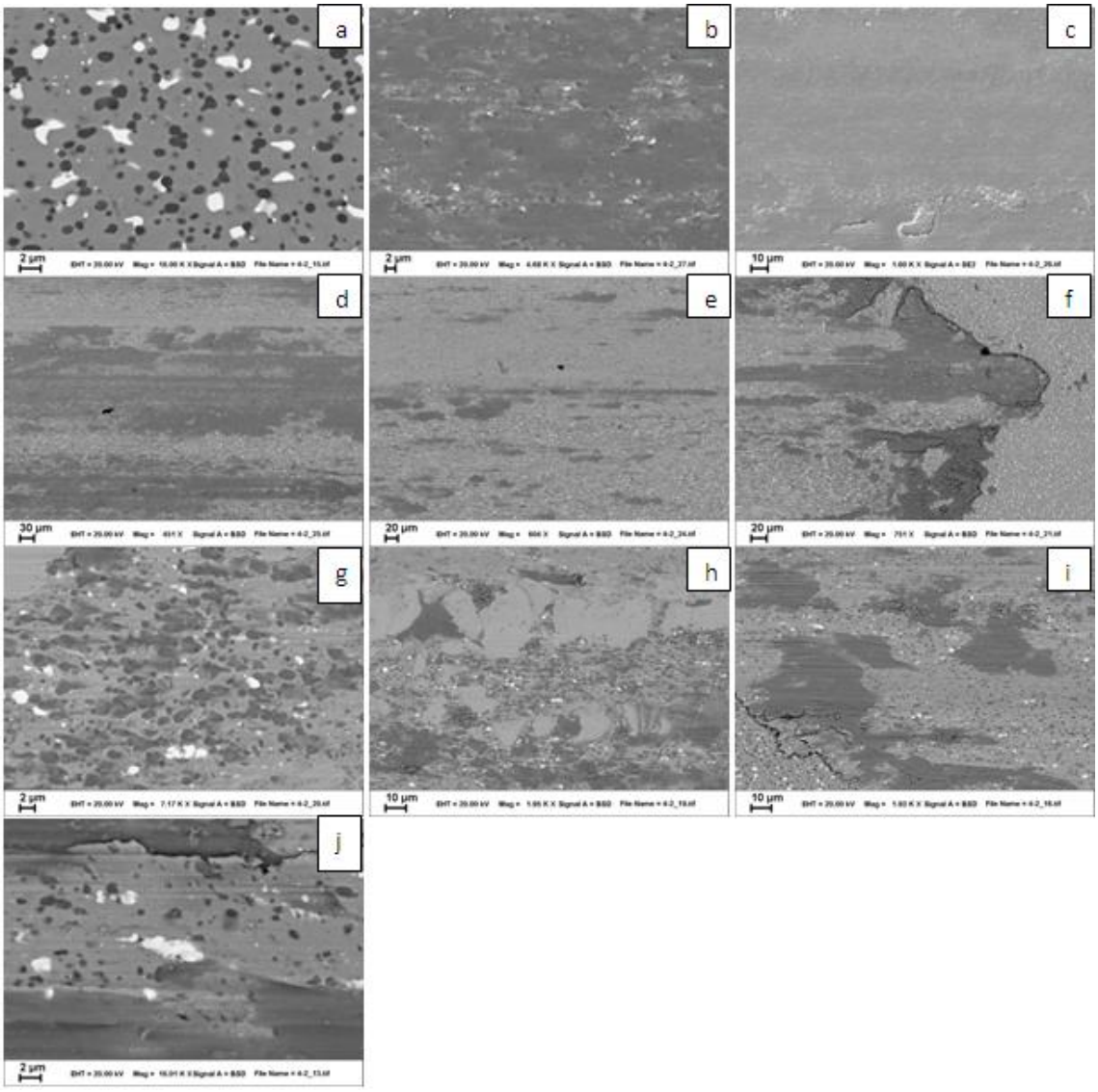

Fig.37: Morphology of S2, High-Load, Dry obtained by SEM

On Fig.37- d, e, i and j the parallel grooves caused by abrasive wear are quite obvious. Also the delamination of oxide layers is recognizable over the surface in mentioned pictures. However it seems smearing is not a dominant issue in this material unlike S1 material with the same test conditions.
By Fig.37-g & j indicate some minor signs of smearing.
There is no sign of glazing.

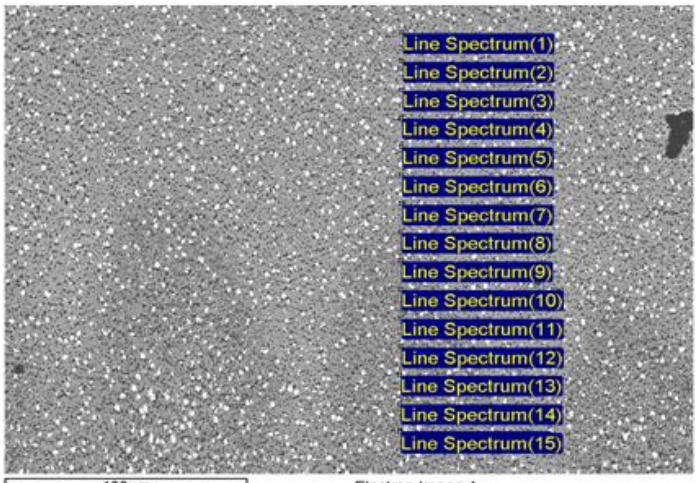

Spectrum	In stats.	C	N	O	V	Cr	Fe	Mo	W	Total
Line Spectrum(1)	Yes	6.14	1.36	1.24	3.93	4.34	78.47	1.80	2.50	99.78
Line Spectrum(2)	Yes	6.48	1.07	1.09	6.47	4.34	76.94	1.86	2.16	100.42
Line Spectrum(3)	Yes	8.28	14.94	2.00	49.91	5.68	19.12	2.55	3.38	105.86
Line Spectrum(4)	Yes	4.77	-0.21	0.95	1.78	4.19	82.52	1.44	1.77	97.20
Line Spectrum(5)	Yes	6.45	0.06	0.93	2.01	4.66	79.04	3.23	4.53	100.91
Line Spectrum(6)	Yes	6.45	1.70	0.96	3.24	4.38	81.64	1.43	1.74	101.54
Line Spectrum(7)	Yes	5.55	3.26	1.12	6.84	4.50	77.33	1.73	2.10	102.43
Line Spectrum(8)	Yes	7.46	1.44	6.00	2.83	4.38	78.42	2.55	3.11	106.19
Line Spectrum(9)	Yes	5.19	-0.47	12.05	3.90	4.43	78.30	1.92	2.32	107.65
Line Spectrum(10)	Yes	8.44	-0.57	9.61	4.90	4.80	77.78	2.10	2.20	109.26
Line Spectrum(11)	Yes	5.53	1.43	13.29	5.53	4.75	72.42	4.26	5.26	112.48
Line Spectrum(12)	Yes	6.00	5.62	13.00	13.80	5.12	67.12	2.23	2.13	115.01
Line Spectrum(13)	Yes	5.77	2.13	6.04	6.94	5.37	73.41	2.32	2.39	104.38
Line Spectrum(14)	Yes	5.19	-0.13	5.04	2.43	4.50	78.91	2.74	2.64	101.33
Line Spectrum(15)	Yes	6.72	2.57	5.43	4.08	4.48	77.54	2.38	3.33	106.52

Fig.38: SEM backscattered image of the micro structure and the chemical composition analysis of 15 different line spectrums on S2 High-Load, Full-Lubricated sample.

In the figure above (Fig.38), Line Spectrums 1 to 7 are taken from the bulk area of the surface and Line Spectrums 8 to 15 are taken from the contact area. The results are indicating that the oxygen content has been increased within the contact area, but obviously not with the same rate as in the non-lubricated sample which is due to the oil layer covering the contact surface and protecting it from oxygen exposure.

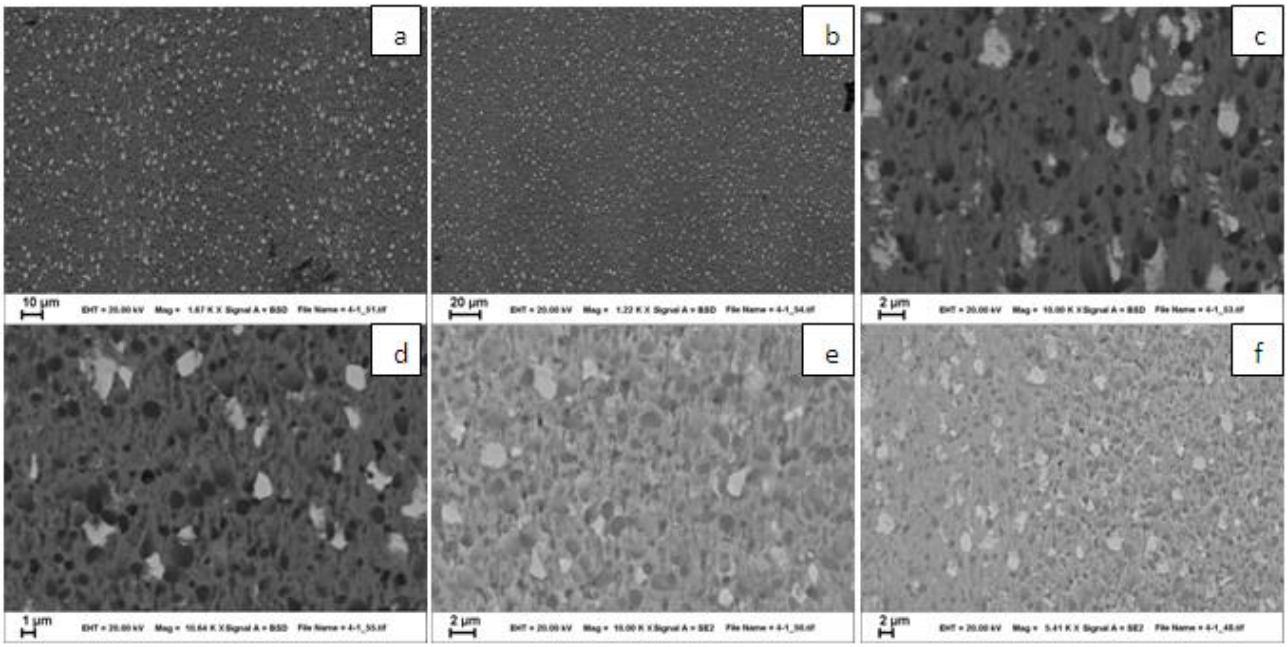

Fig.39: Morphology of S2, High-Load, Full-Lubricated obtained by SEM

Here in Fig.39 no signs of loose particle, abrasive wear or glazing are observed. Smearing is not indicated in the figure above while in Fig.41 some minor signs of smearing are recognizable.

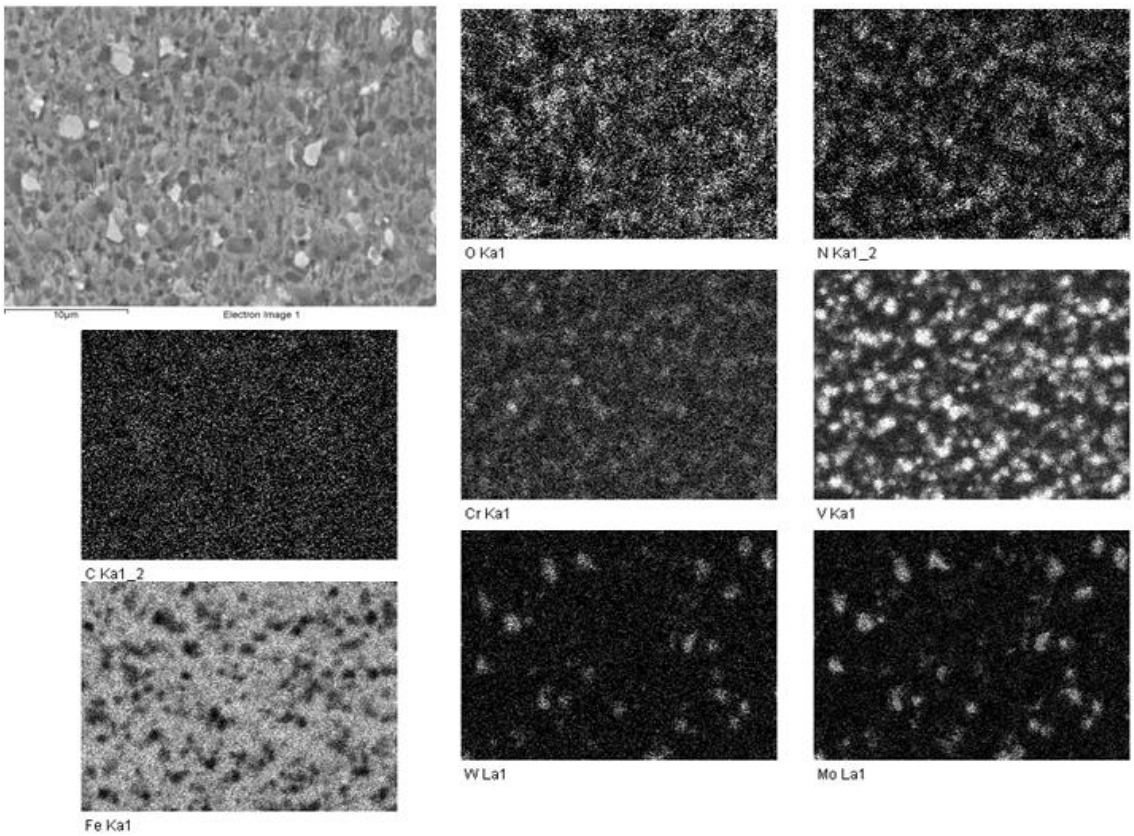

Fig.40: SEM image and X-ray elemental mapping of the wear track of S2 with High-Load, Full-Lubricated condition, taken from a dark region over the contact surface.

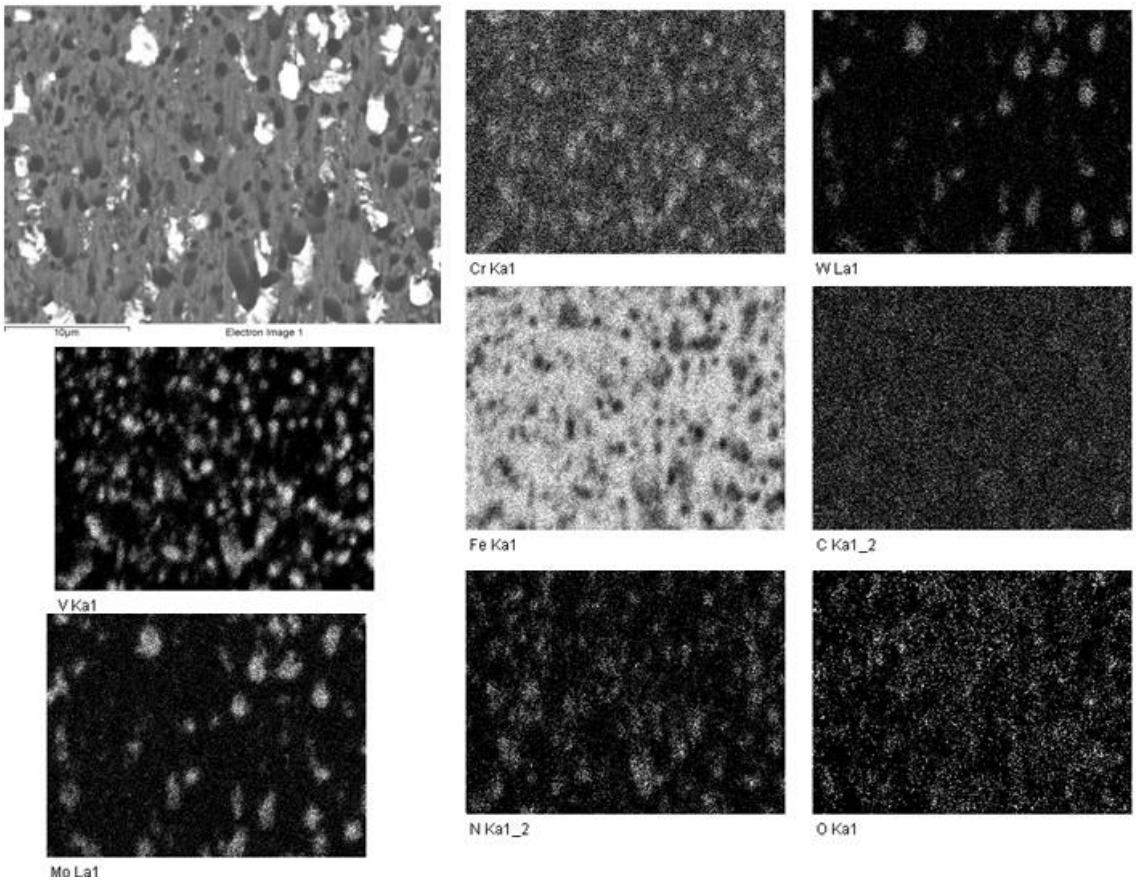

Fig.41: SEM image and X-ray elemental mapping of the wear track of S2 with High-Load, Full-Lubricated conditions, taken from a bright region over the contact surface.

5.3 S3

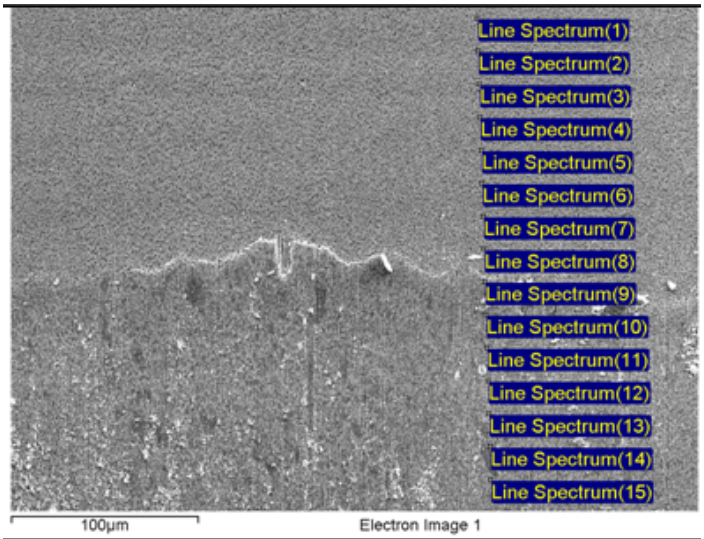

Spectrum	In stats.	C	N	O	V	Cr	Fe	Mo	W
Line Spectrum(1)	Yes	40.76	-7.75	7.15	4.49	3.09	51.26	0.85	0.14
Line Spectrum(2)	Yes	42.84	-10.45	7.78	2.64	3.04	53.18	0.77	0.19
Line Spectrum(3)	Yes	38.79	-1.53	10.97	9.52	2.91	38.49	0.66	0.20
Line Spectrum(4)	Yes	43.41	-7.41	5.67	3.96	3.02	50.32	0.81	0.21
Line Spectrum(5)	Yes	42.06	-6.74	9.24	9.44	3.13	41.96	0.72	0.18
Line Spectrum(6)	Yes	43.81	-4.43	5.35	3.79	2.79	47.81	0.70	0.19
Line Spectrum(7)	Yes	37.95	2.71	10.89	10.04	2.70	34.78	0.73	0.20
Line Spectrum(8)	Yes	1.45	-0.16	3.29	26.89	5.59	61.72	0.74	0.50
Line Spectrum(9)	Yes	32.13	14.71	16.76	17.86	2.45	15.53	0.46	0.10
Line Spectrum(10)	Yes	41.60	6.08	9.94	6.64	2.30	32.66	0.66	0.12
Line Spectrum(11)	Yes	15.54	-1.03	37.50	3.94	2.52	40.65	0.67	0.21
Line Spectrum(12)	Yes	25.09	2.47	17.98	7.24	2.92	43.32	0.79	0.20
Line Spectrum(13)	Yes	31.85	14.60	12.94	12.88	2.48	24.58	0.53	0.13
Line Spectrum(14)	Yes	8.58	3.23	39.33	15.15	2.93	29.85	0.73	0.20
Line Spectrum(15)	Yes	28.40	-1.23	38.30	7.52	1.98	24.47	0.47	0.10

Fig.42: SEM backscattered image of the micro structure and the chemical composition analysis of 15 different line spectrums on S3 High-Load, Dry sample.

The figure above (Fig.42) indicates the line spectrum analysis of the S3 material in high load non-lubricated test taken from 15 different points including non-contact surface and contact surface of the sample from the contact start line. The oxygen content increases by moving further into the contact zone such that we see it is growing from 7% at the line spectrum1 to about 39% at the line spectrum15.

Loose particles are seen all over the contact surface including dark oxide layers. In figure below we examine the dark layers chemical composition and we find extreme increase in oxygen content which is over 50% all over. These dark oxide layers are departing from the surface and replacing with new oxides. This seems to be the major wear mechanism.

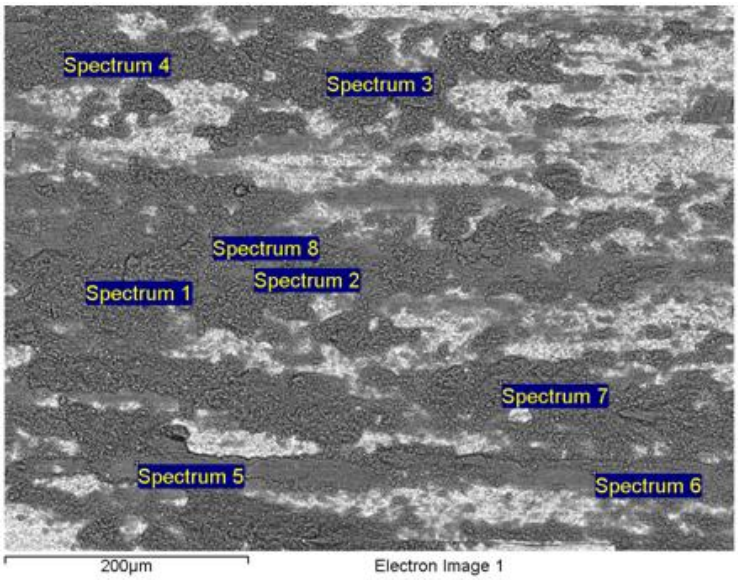

Spectrum	In stats.	C	N	O	V	Cr	Fe	Mo	W
Spectrum 1	Yes	9.82	2.84	58.65	3.90	1.51	22.61	0.53	0.14
Spectrum 2	Yes	9.13	4.39	46.57	8.65	2.19	28.29	0.63	0.16
Spectrum 3	Yes	9.32	3.47	48.36	5.05	2.04	30.89	0.69	0.17
Spectrum 4	Yes	9.91	2.46	55.95	3.71	1.60	25.61	0.59	0.17
Spectrum 5	Yes	9.08	3.29	48.12	5.29	2.54	30.80	0.67	0.21
Spectrum 6	Yes	7.14	2.53	51.18	6.81	2.14	29.38	0.67	0.16
Spectrum 7	Yes	10.33	2.88	53.53	4.53	1.83	26.21	0.55	0.15
Spectrum 8	Yes	7.99	4.07	52.18	9.31	2.00	23.70	0.61	0.14

Fig.43: SEM backscattered image of the micro structure and the chemical composition analysis of 8 different spectrums on contact surface of S3 sample of High-Load, Dry taken from the dark regions.

The dark layers are obviously separate from the bulk material below and building up the loose particles over the surface which will be easily removed by getting robbed by the competing surface against it.

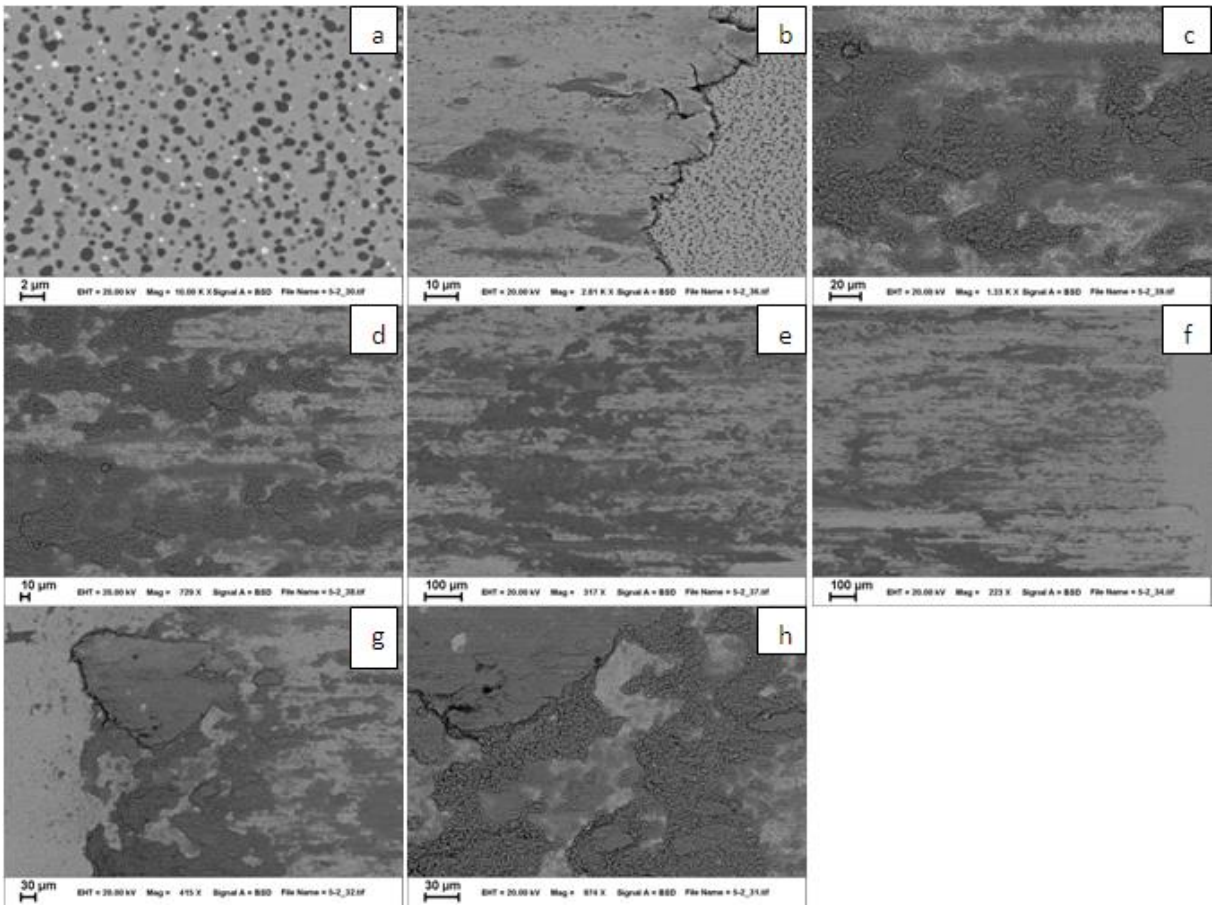

Fig.44: Morphology of S3, High-Load, Dry obtained by SEM

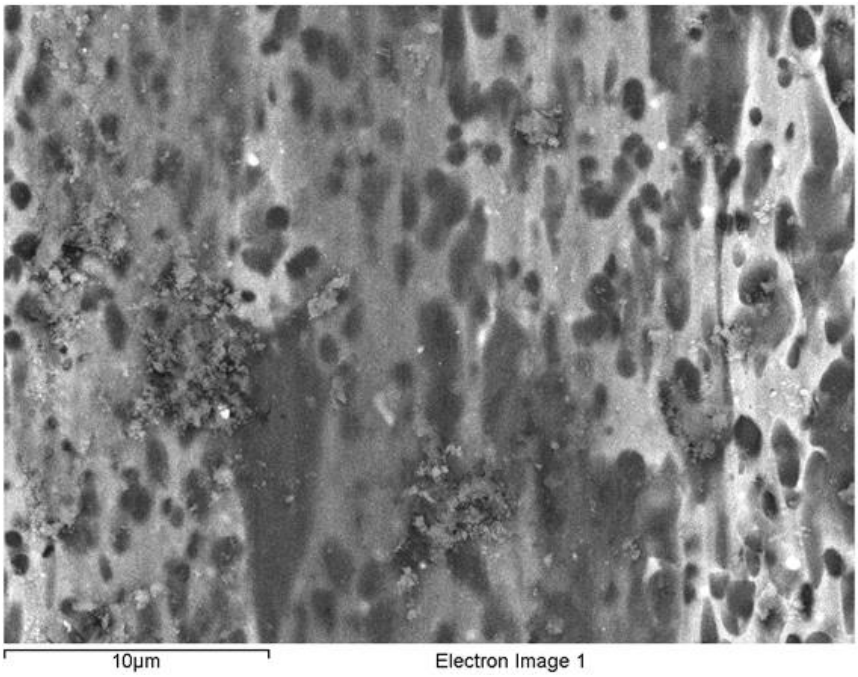

Fig.45: Morphology of S3, High-Load, Dry obtained by SEM

Fig.45 illustrates the contact surface of the high load non-lubricated sample of the S3, in which minor indications of smearing is observed. Also loose particles are all over which earlier we examined some of them and we found them as oxides.

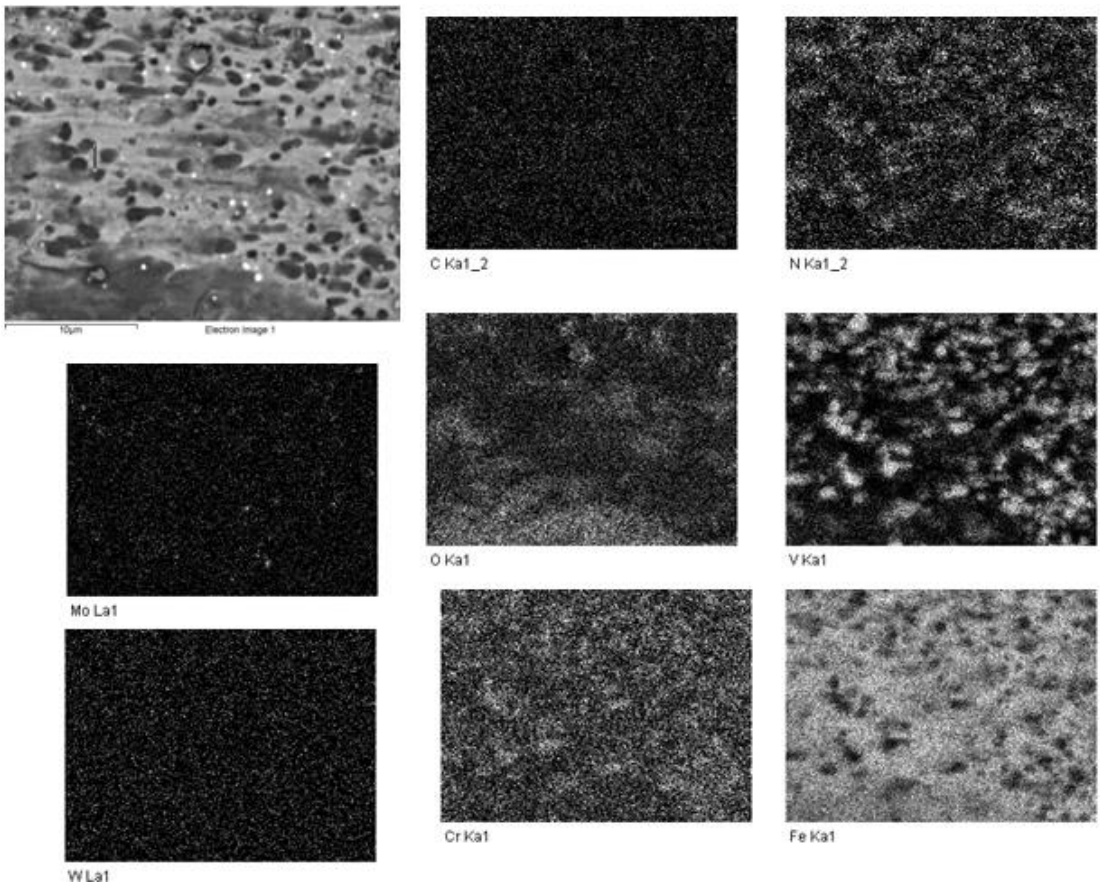

Fig.46: SEM image and X-ray elemental mapping of the wear track of S3 with High-Load, Dry conditions, taken from the contact surface.

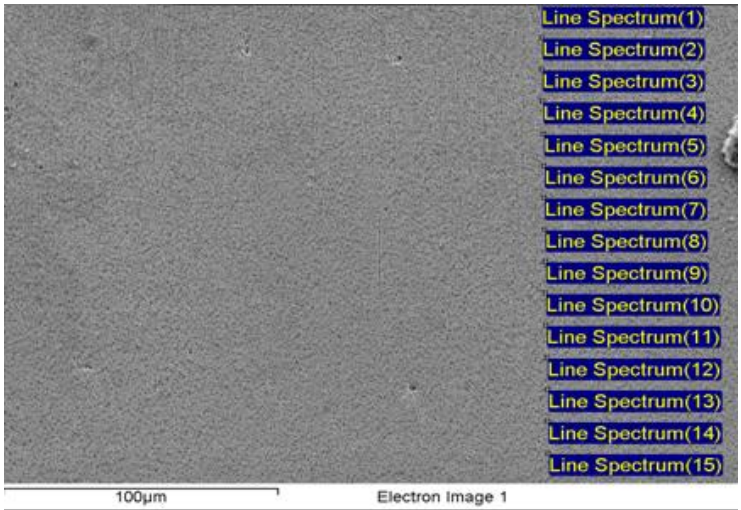

Spectrum	In stats.	C	N	O	V	Cr	Fe	Mo	W
Line Spectrum(1)	Yes	17.58	5.48	20.28	4.45	3.03	48.06	0.86	0.26
Line Spectrum(2)	Yes	12.11	5.99	35.00	6.84	2.76	36.33	0.81	0.16
Line Spectrum(3)	Yes	24.82	0.53	21.16	2.36	2.83	45.13	2.65	0.51
Line Spectrum(4)	Yes	21.11	-0.40	10.08	2.47	3.45	62.16	0.88	0.24
Line Spectrum(5)	Yes	20.11	5.86	14.52	7.31	3.09	48.09	0.79	0.23
Line Spectrum(6)	Yes	16.43	23.55	15.14	24.15	3.12	16.88	0.61	0.13
Line Spectrum(7)	Yes	18.19	11.59	20.00	5.85	2.63	40.81	0.75	0.18
Line Spectrum(8)	Yes	20.21	19.94	7.89	11.03	2.98	36.94	0.81	0.20
Line Spectrum(9)	Yes	18.13	2.97	14.61	5.55	3.31	54.08	1.07	0.28
Line Spectrum(10)	Yes	19.68	3.34	14.75	11.15	3.28	46.53	0.98	0.28
Line Spectrum(11)	Yes	16.97	4.21	18.11	3.98	2.85	52.72	0.91	0.27
Line Spectrum(12)	Yes	16.82	11.54	8.34	12.79	3.64	45.88	0.84	0.14
Line Spectrum(13)	Yes	16.46	9.64	5.02	12.93	3.70	51.02	1.00	0.24
Line Spectrum(14)	Yes	20.12	17.53	5.27	15.34	3.16	37.60	0.84	0.14
Line Spectrum(15)	Yes	18.78	13.36	3.59	9.28	3.50	50.48	0.77	0.24

Fig.47: SEM backscattered image of the micro structure and the chemical composition analysis of 15 different line spectrums on S3 High-Load, Fully-Lubricated sample.

The figure above shows that the surface of this sample has not been oxidized as much as others which mean that the surface has got a better protection from exposure to the air so that oxygen has not been able to penetrate through the oil film.

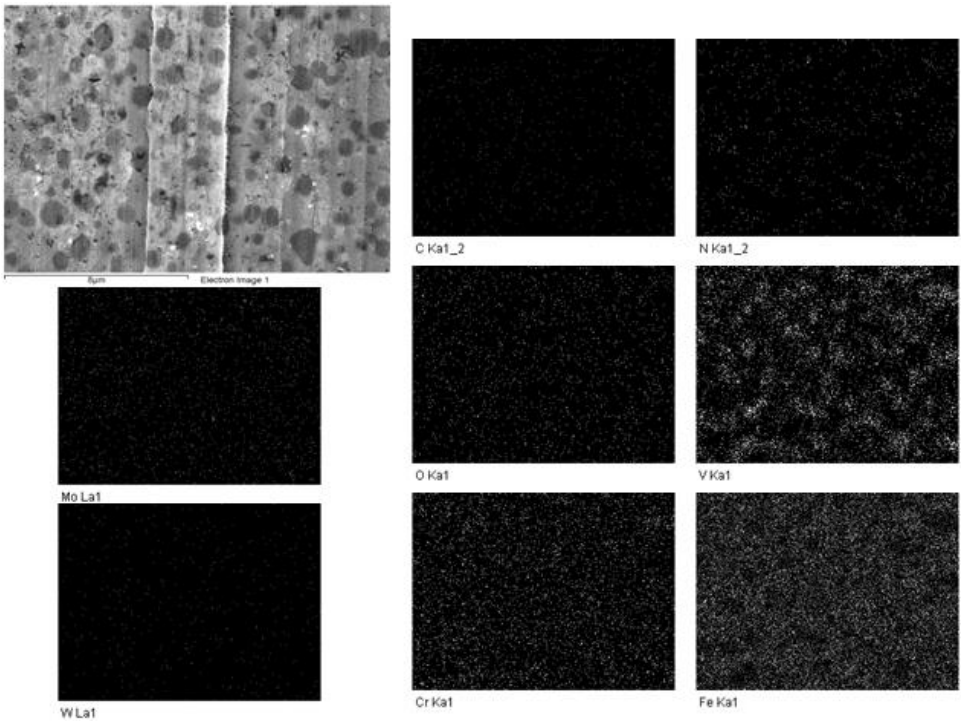

Fig.48: SEM image and X-ray elemental mapping of the wear track of S3 with High-Load, Full-Lubricated condition.

The Fig.48 indicates the result of the elemental mapping made to illustrate the average chemical composition.

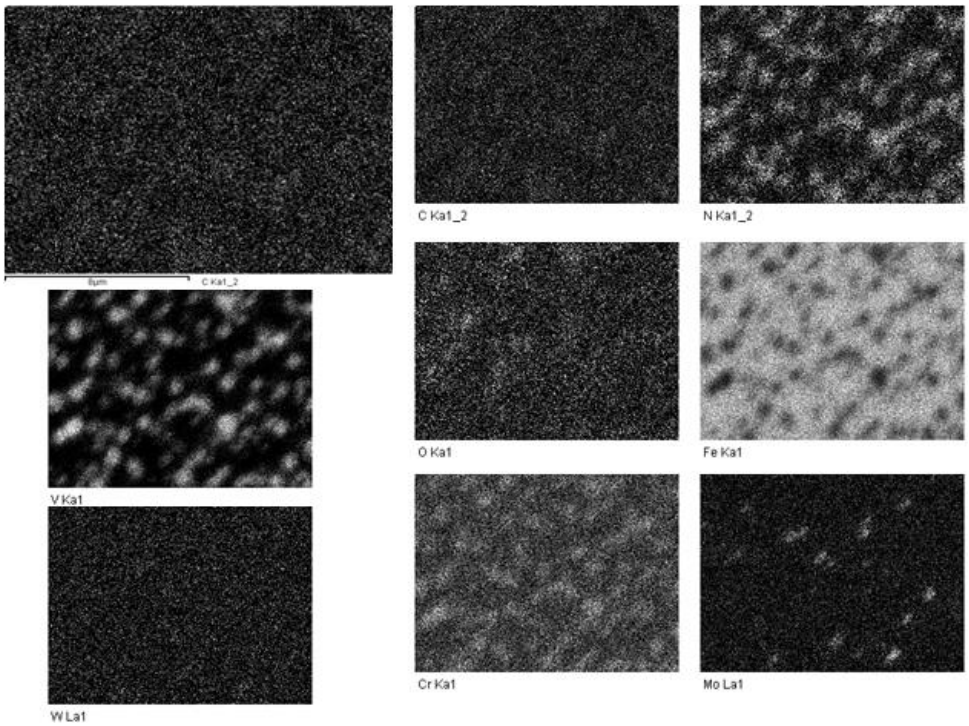

Fig.49: SEM image and X-ray elemental mapping of the wear track of S3 with High-Load, Full-Lubricated condition (taken from the same area as in Fig.48.

Fig.49 indicates the result of the elemental mapping taken from the same area as in Fig.48 to illustrate the phases.

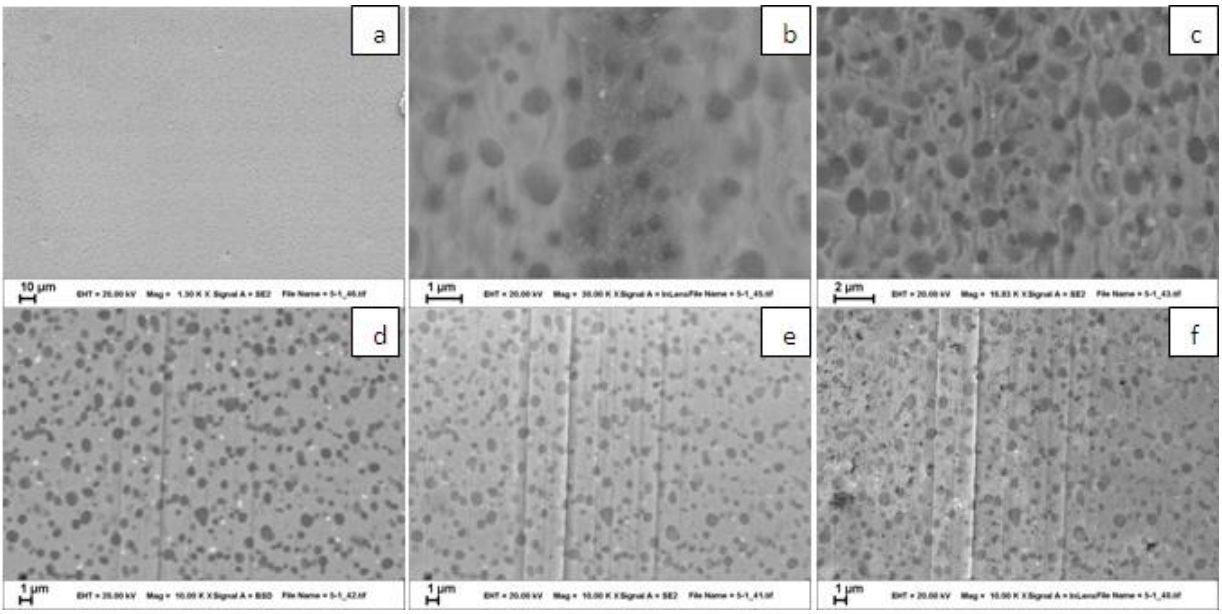

Fig50: Morphology of S3, High-Load, Full-Lubricated obtained by SEM

6. Discussion

6.1 Loads vs. Temperatures

On non-lubricated samples, the load range affected the temperature so that the higher the load was the more the temperature increased which is clearly due to the friction rate.

Increasing the load for the full-lubricated condition does not force any considerable raise in the temperatures and this is because of the controlled friction due to the lubricant film between the two metallic surfaces and also the cooling effect of the lubricant. Therefore the temperature at the contact area does not raise more than a certain rate.

However in the poor-lubricated condition the lubricant film is not as effective as full-lubricated tests, the temperature is still controlled and we do not see considerable changes in temperatures up to a certain load range. But above this range we observe considerable changes, i.e. here the temperature with the highest testing load is about 20% higher than the temperatures registered in lowest load.

6.2 Test Period

By the non-lubricated sliding test of steels, the area of the surface covered by oxide layer will depend on test duration; meaning that the longer the test lasts the wider contact area will be covered by oxide film. There other factors which influences this fact as sliding speed and load. We also know that during the test, some parts of oxide layer will be removed by friction between two sliding surfaces. [6]

Oxide films get cracked and broken and result in loose particles on the surface that will spall off and become debris with sharp edges which will increase the friction and wear of the surfaces. [7]

6.3 Temperature

As we mentioned earlier, Vanadium Magneli phases would appear over the contact surfaces of the samples in temperatures over 500°C and in that temperature range they appear to be very effective in decreasing the friction rate [30, 35-37].
In lubricated test we are in fact preventing the contact surfaces from exposing with the surrounding air which will pretty much explain the lack of tribo layers over the contact surfaces. But with the non-lubricated tests since we are exposing the contact surfaces with the air, it seems like there are other reasons why we do not find tribo oxides especially Magneli phase, and that can be explained by the above mentioned phenomena; since the tests were applied in room temperatures, the surfaces never achieve that high enough temperatures to be sufficient to create tribo layers as Magneli phase or glazed surface.

6.4 Load

By increasing the load in absence of lubricant, up to a certain level of loading, the wear rate does not show significant changes and it rises considerably after that while in presence of lubrication regardless of having it poor-lubricated or full-lubricated, the changes in the load do not cause much change in the wear rates.

6.5 Friction Coefficient

6.5.1 Full-Lubricated

6.5.1.1 High- Load

For the highest load tests all three materials rising up sharply at the beginning but then S1 and S2 continue with a very gradual fall in the values such that within over 380m of sliding distance the CoF values sink for about 0.02, while S3 follows a gradual rising trend with some fluctuations for the CoF value during test and ends up at some 0.02 higher value.

6.5.1.2 Mid-Load

The CoF of S1 in mid-load test rises fast at the beginning of the test as in the test with the highest load but the maximum achieved value here is about 10% less than the test with the highest load test. After the maximum point, the CoF value starts falling as in the highest load test but faster such that the CoF decreases about 0.05 after the same sliding distance. With the same conditions S2 shows a slightly different trend from the test with the highest load. Here we see that the CoF rises up and achieves a 20% higher value and again falls sharply to 20% less than highest load test which is almost the same value as for S1 in this test and then continues around the same value with some unstable fluctuations and finally ends at the same level after 400m of sliding distance.
S3 but in the mid-load achieves 40% higher as maximum value compared with its maximum value in highest load test and sharply falls to the same value as the maximum value in highest load test. After this it follows a gradually sinking trend but never reaches less than 10% below that value and suddenly after about 380m sliding distance it rockets up.

6.5.1.3 Low-Load

Low-load tests of three samples show that S1 starts and ends around the same level (~0.25) with some moderate fluctuations and gradual changes during the test.
S2 but shows a very unstable result such that the values sharply rise and fall several times during the test. However the trend shows a very gradual decrease in the values.
With the same conditions S3 behaves differently. It shows drastic fluctuations and very sharp rises and falls. Also the general trend has an irregular downwards slope.

The lubrication effect on the CoF is obvious in the all three test results that the samples are having low CoF values and this value not only does not increase but even for S1 and S2 we

see that it slightly falls during the test and this is caused by that the two sliding surfaces polish each other on the sliding track while the lubricant acting in between. The lubricant is acting as a protective substance on the surface to avoid the air/oxygen to contact the surface and penetrate through and react with the material and oxidize it.

6.5.2 Poor-lubrication

- By the high-load tests all three materials start with CoF values of below 0.2 and follow a rising trend with some unstable fluctuations but at some certain points they rocket up and there we stop the test. Here we see that S1 lasts for less than 200m before this point while S2 lasts up to 400m and S3 shows even a better quality by lasting over 500m.
- Mid-load test for S1 shows that the CoF starts slightly over 0.1 and sharply rises up to 0.3 but then it follows a stable horizontal trend and it starts rising after about 380m. With the same conditions for S2 and S3 follow more or less flat trends with very minor fluctuations but then they rocket up at some certain points as we saw in high-load tests. There are some major differences between S2 and S3 here. One is that S2 starts with a CoF of about 0.25 while S3 starts at 0.15. The other thing is that S2 lasts for about 120m before the CoF rockets up while S3 lasts for more than 420m of sliding distance before this point. Here also we see S3 gives a better performance and lasts longest among all three samples.
- S1 in low-load test shows a very unstable trend and rockets up after just 30m of sliding distance. This did not comply with the expectations. S2 but lasts over 400m sliding distance however shows several unstable fluctuations and ends up to a CoF value which is close to the start value. S3 on the other hand shows a moderate rise at the beginning of the test but then after about 50 meters follows a falling trend down to a CoF value which is about the same start value within about 400m.

In this final test, I have no proper explanation for the result achieved from S1 but on the other hand we see that S2 and S3 last longer than they did on high-load and mid-load and this proofs the effect of load rate on the friction and wear of the materials in poor lubricated conditions.

6.5.3 Dry

- We see pretty different results for our three samples in non-lubricated tests with the highest load.
  S1 starts with a CoF of 0.5 and continues rising but just after 60m sliding distance rises straight up to over 1 and continues up where the test is stopped. S2 but starts at a CoF of 0.2 and rises fast up to over 0.6 and follows an unstable but even trend and finally after about 250m of sliding distance starts rising drastically and that's where the test is completed.

And finally S3 starts with about 0.5 and follows down a very unstable trend to achieve a CoF value of about 0.2 after more than 220m and there it rises straight up.

- By the mid-load S1 shows a rising trend in which it starts at 0.4 and reaches 0.8 after 30m where it falls for about 20% and rises up right away and the test is held just for 40m.
  S2 but follows a gradual rising trend between 0.6 and 0.75 within 30m sliding distance where it suddenly rises up.
  S3 then starts at 0.3 and rises rapidly up to 0.9 in about 100m where it starts rising sharp up.
- S1 at the low-load test follows a rising trend between 0.4 and 0.8 within less than 30m sliding distance and then rises sharp up.
  S2 then starts with 0.5 and rises up to 0.8 in about 50m and then it continues with an even trend with no considerable changes for about 900m.
  S3 starts with 0.5 and gradually rises up to 0.8 within about 100m and there it rockets up.

In dry tests S1 is showing very alike results for low-load and mid-load, but still the mid-load sample lasts about 30% longer while the high-load sample shows a better result by lasting a about 100% longer than low-load.

S2 shows a relatively long life time by the high-load test but the result from the low-load is unexpected. One possible explanation for this result can be that the hard oxide layer formed on the surface and the normal load is not enough to break this layer massively and create the debris at the contact surface so that increase the friction.
However this condition is not seen on two other samples.

S3 has the best result with the high-load, the mid-load sample last half the sample in high-load and the low-load sample last 10% shorter than the mid-load.
This seems to be due to oxidation rate. The higher the load is the higher the temperature is at the contact surface therefore the oxidation rate will be higher so the metal-metal contact is better prevented.

6.5.4 CoF vs. Lubrication

6.5.4.1 Full-Lubricated

By the first look we see that the CoF graphs for all three materials are having similar starting points and following with similar behavior such that the CoF decreases.
This is due to the fact that the lubricant is protecting the surface from the free air exposure and oxidation. And a well-known phenomenon by which the sliding surfaces polish each other in presence of lubricant so that the contact surfaces become smoother and reduces the friction.
As we mentioned above this effect is seen in all three samples in all different loads.

6.5.4.2 Non-Lubricated

Oxidation is a very basic result of the lack of protection against the air. As we discussed earlier in this paper, oxidation (especially in relatively low temperatures) forms brittle and normally unstable oxide layers over the contact surface which will later be removed and cause a wear mechanism which we referred to it as oxidational wear.
The oxide layers, besides the brittleness and relative frangibility and instability, are low friction layers.
The process of formation and removal of these low friction layers appear as raise and falls in the CoF graphs as we observe in all three materials in different load rates until the samples get into the seizure level and the CoF rockets up which is the point where we stop the test.

As we can see in the test results S1 samples last least in all three tests compared with two other samples, S2 and S3, in the same conditions while the samples of these two materials show similar life time rates which are relatively longer than the ones S1 gives.

6.5.4.3 Poor-Lubricated

In the Poor-Lubrication conditions the behavior and the life time of the samples has signs of both Full-Lubrication and Dry conditions but do not follow either of them completely. The samples get to seizure as in dry conditions and also we see that the changes in CoFs are not as regular as in Full-Lubricated samples and still the instabilities are not as savior as Dry tested samples. And also the life times before the seizure are way longer than the same samples and conditions in Dry tests while the Full-Lubricated samples did not get to the seizure.
This shows that this limited amount of lubricant is partially preventing the contact surfaces from direct (metal-metal) contact and exposure to the air which results in relatively less friction and oxidation compared with Dry conditions, but still not as good lubrication effect as in Full-Lubrication conditions.

S3 gives longer life times and better performances compared to the S1 & S2 in this condition, especially with low load in which S3 does not got to the seizure mechanism.

6.6 Wear rates

6.6.1 High-Load

6.6.1.1 Full-Lubricated

Despite all three of the samples show closely similar temperatures and CoF rates S1 wears most followed by S2 and S3 stands on the third place in this test.
On one hand we know that S1 is a Nitrogen free alloy while S2 and S3 are Nitrogen alloys and also we know that the nitrogen content of S3 is about 30% more than the Nitrogen content of S2. The Nitrogen content rate can be one of the main factors which explain the differences in the wear rates and wear resistance of Nitrogen alloys here.

No sign of seizure or oxidational wear is seen at this test which means there has not been any metal-metal contact. This is expected since the contact surfaces are lubricated so that the lubricant prevents the surfaces from direct contact. [9]

On the other hand by comparing the hard phase inclusions of the sample materials we see that the hard phases in S1, S2 and S3 include 16%MC+7%M7C3, 14%MN+5%M6C and 19%MN respectively. Besides the Nitrogen content, MN hard phase might play an effective role in reducing the ware rates of the materials in applications with decent lubrications, which is causing S3 with the most MN phase wears least and S1 with no MN phase wears most in our test.

Due to the proper lubrication applied on theses specimens, the friction is low and no sign of seizure or severe wear have been observed. These are all results of metal sliding on metal without lubrication. [23] The wear here is mild abrasive wear.

6.6.1.2 Dry

Here S2 wears most, S1 stands on the second place and S3 wears least. However S2 and S3 benefit from the Nitrogen content effect and not S1, still S1 is worn more than S3 which with more investigations, might prove that there are other factors affecting the wear rates.

In addition the hard phases in these three samples show a slightly different effects in Dry conditions compared with lubricated conditions. It seems like MN phase which is the main hard phase in S3 is still making an effective contribution in the lack of lubricant for S3 but not for S2. The consequent of the Combination of MC and M7C3 phases in S1 is showing a better effect compared with the Nitrogen content and the hard phase in S2 in the lack of lubricant.

These three samples with high friction, seizure and severe wear over the contact areas including severe abrasive wear and mild oxidational wear as dominant wear mechanisms respectively. [16]

6.6.1.3 Poor-lubricated

S1 is worn most which lack of Nitrogen content and MN phase can be main causes of it but S2 is worn less than S3 while S3 contains about 30% more Nitrogen and more MN phase, therefore there might be some other dominating factors that are effective here which need more investigations.
On the S3 sample surface we see that seizure has occurred at a certain area. This means metal-metal contact has happened due to poor separation by the lubricant. [27] This can explain the reason why S3 shows a higher wear rate here in this test.

6.6.2 Mid-load

6.6.2.1 Full-Lubricated

S1 wears least and S3 wears most in this test. A sign of seizure is seen on a small area on S3 sample.
This is an unexpected matter since we have applied continuous lubrication during this test. This might have happened due to some external causes as extra debris trapped between the surfaces so that caused unexpected wear over the contact surface of the sample.

6.6.2.2 Dry

Signs of seizure are seen on all three samples while S1 and S2 samples have severe seizure signs and we have relatively less seizure occurred on S3 compared with S1 and S2. The seizure is occurring at the load concentration areas much more than areas around and this is a well-known phenomenon. S1 is having the largest worn area among all three.

The hard phase of the S3 should be a key player here as well.

6.6.2.3 Poor-Lubricated

Here also we see some minor seizure signs again on S3. The seizure proves the lack of decent lubrication to separate the metallic surfaces and prevent the severe wear.

S2 is worn most and S3 least.

This is pretty much the same situation for S3 as we saw in High-Load test with the same lubrication condition which can be explained by the Nitrogen content and the hard phase arrangements.
But here S1 has worn less than S2 which in the High-Load test it happened the other way around. Therefore there should be other players ruling the results.

6.6.3 Low-load

6.6.3.1Full-lubricated

There are some minor signs of seizure on S1 sample which does not make sense since we have applied a continuous lubrication during the test and this is not expected to occur. S2 and S3 show a very smooth worn areas as we expected while S2 has the largest worn area among all three samples and S1 has the least worn area but with some severe wear signs as we mentioned above.

6.6.3.2 Dry

All three samples have seizure signs over the contact areas. S2 has the maximum wear rate S1 has minimum, which is totally unexpected.

6.6.3.3 Poor-Lubricated

On these samples we see no seizure and S2 shows the most wear rate and S3 least.

6.7 CoF & Sliding distance Vs Wear rates

6.7.1 High-Load

Among the full-lubricated samples S1 gives the largest worn area whilst lowest average CoF. S3 here has the smallest worn area and highest average CoF. All three test samples have been running for the same sliding distance and did not get to the seizure.

The results registered from the Dry tested samples give a different pattern such that the S2 with over 250m sliding distance gives the largest worn area and S1 wear rate stands in the second place with 10% less wear rate compared to S1 while it has slide just 60m with the highest average CoF among all. S3 then runs the same distance as S1 and wears least and shows less CoF average.

With the Poor-Lubrication tests we see that all the samples start to seizure at some point. Here S1 runs less than 200m before it gets to seizure with the highest CoF average and the largest worn area while S3 gets to the seizure after over 600m and a wear rate of 10% less. S2 here seizures after about 450m which is about 25% shorter sliding distance compared to S3 when its wear rate is about 19% of the S3, which means that S3 is giving the best performance regarding the wear rates and S1 has the worst overall performance under high loads.

6.7.2 Mid-Load

Here we see that S3 is the only sample among the full-lubricated samples which gets to the seizure level which was not expected. Therefore something unpredicted must have happened between the sliding parts for S3 such as some extra debris, so we disregard the result gained from this material in this condition. Between S1 and S2 it is S2 with a higher wear rate which is about 5% more than the wear rate in the S1 while we do not see a considerable difference in average CoFs.

Dry test results show that the S3 wears less than two other materials. It is more than 10% less than the wear rate in S1 and about 3.5% less than the wear rate in S2 while it slides 200% longer than S1 and 300% longer than S2 before it starts to seizure. S1 and S2 give almost the same CoF average and S3 has about 25% smaller CoF average compared to the S1 and S2.

Poor-lubricated samples give pretty much the same results as the Dry tested samples, such that S3 wears 10% less than S1 and 15% less than S2 while sliding about 50% more than S1 and about 200% more than the S2 sample. This is whilst the average CoF of the S3 test (0.18) is considerably less than S2 (0.25) and S1 (0.28).

6.7.3 Low-Load

S1 full-lubricated, low-load sample gives the least wear rate followed by S3 sample with less than 5% bigger worn area while the CoF average of S3 is about 18% less than the S1 sample. S2 is worn most with almost the same average CoF S1. All three tests held the same length and none of the samples seizure.

With the dry samples S1 and S2 run in a range of CoFs which are close to each other but S1 starts to seizure after less than 30m of sliding distance where S2 lasts for about 100m before it seizures and wears 77% more than S1. S3 but with sliding distance and CoF range that are partially the same as S2 sample, gives 15% less wear rate compared with S2.

Poor-lubricated S1 starts to seizure after 30m sliding while S2 and S3 do not get to seizure level even after 400m sliding which is the test limit. S2 here wears most with the highest CoF range where S1 wears 30% less but with a CoF range which is 75% less S2 sample, and a very short sliding distance as mentioned above. On the other hand we have S3 which runs the same distance as S2, with a CoF range which is about 40% less and wears about 43% less than S2.

7. Conclusions

[1] Load rate in non-lubricated conditions does not affect the wear rate much before it reaches to some relatively high levels.

[2] The changes in the load do not cause much change in the wear rates in lubricated conditions.

[3] Changes of CoF for the S1 (Nitrogen free PM tool steel) follows pretty much the same trend in non-lubricated conditions for different loads.
S2 and S3 show more stable CoF results in lower loads and less CoF values by higher loads which are still not considerable.

[4] However the adhesion is not detectable by EDX chemical composition analysis due to the fact that both test cylinders and blocks are made of the same materials, in the SEM pictures we do not see any microscopic signs of adhesion which is referred as galling in any of the samples.

[5] We do not observe any protective low friction tribo layers as glazing or tribo oxides over the contact surfaces of any samples.

[6] Nitrogen content and hard phases in the alloys has direct effect on the wear rates. Such that samples with more Nitrogen content are more wear resistant and also the composition and type of hard phase has a great influence on wear rates.

[7] Lubrication quality has direct effect on wear rates and wear mechanisms.

8. Reference

[1] Krauss G. Steels. Processing, Structure, and Performance, ASM International, Materials Park, Ohio 2005;

[2] Corrosion and wear resistant nitrogen alloyed steels by Uddeholm]

[3] O. Sandberg, L. Westing, Powder metallurgy manufactured high speed, in US Patent 2004, Uddeholm Tooling Aktiebolag, Erasteel Kloster Aktiebolag.

[4] T.F.J Quinn, The Thermal aspects of wear in tribotesting, Proc.Instn. Mech. Engrs. C183/87 (1988) 253-259

[5] T.F.J Quinn, Oxidational wear modeling (Part I), Wear 153 (1992) 179-200.

[6] T.F.J Quinn, Oxidational wear modeling. Part II: The general theory of oxidational wear, Wear 175 (1994) 199-208.

[7] T.F.J Quinn, Oxidational wear modeling. Part III: The effects of speed and elevated temperatures, Wear 216 (1998) 262-275.

[8] S.C. Lim, M.F. Ashby, Wear-mechanism maps, Acta Metall. 35 (1987) 1-24.

[9] H. So, D.S. Yu, C.Y. Chuang, Formation and wear mechanism of tribo-oxides and the regime of oxidational wear of steel, Wear 253 (2002) 1004-1015.

[10] T.F.J Quinn, Review of oxidational wear. Part II: Recent developments and future trends in oxidational wear research, Tribol. Int. 16 (1983) 305-351.

[11] T.F.J Quinn, Oxidational wear, Wear 18 (1971) 413-419.

[12] T.F.J Quinn, Review of oxidational wear. Part I: The origins of oxidational wear, Tribol. Int. 16 (1988) 71-75.

[13] Archard JF, Hirst W. The wear of metals under unlubricated conditions. Proc R Soc 1956; A236:397-410.

[14] Archard JF, Hirst W. An examination of a mild wear process. Proc R Soc 1957; A238:515-28.

[15] Suh NP. The delamination theory of wear. Wear 1973; 25:111-24.

[16] Lim SC, Isaacs DC, McClean RH, Brunton JH. The unlubricated wear of sintered steels. Tribo Int 1987; 20:144-9.

[17] Lim SC, The relevance of wear-mechanism maps to mild-oxidational wear, Trobol. Int. 35 (2002) 717-723.

[18] Quinn TFJ. The role of oxidation in the mild wear of steel. Br J Apple Phys 1962;13:33-7.

[19] William K, Giffen E. Friction between unlubricated steel surfaces at sliding speeds up to 750fft/s. Proc. I Mech E 1963-64; 178(3(N)):24-36.

[20] Earles SWE, Kadhim MJ. Friction and wear of unlubricated steel surfaces at speeds up to 655ft/s. Proc. I Mech E 1965-66; 180:531-47.

[21] Powell DG, Earles SWE. Wear of unlubricated steel surfaces in sliding contact. ASLE Trans 1968;11:101-8.

[22] L. Rapoport. The competing wear mechanisms and wear maps for steels; Department of Mechanics and Control Center for Technological Education Holon, PO Box 305, Holon 58102, Israel

[23] Modern Tribology handbook, Bharat Bhushan

[24] O. Sandberg, L. Westin, Power metallurgy manufactured high speed steel, in US Patent 2004, Uddeholm Tooling Aktiebolag, Erasteel Kloster Aktiebolag.

[25] Sepehr Hatami, Alexandra Nafari, Lars Nyborg, Urban Jelvestam. Galling related surface properties of powder metallurgical tool steels alloyed with and without nitrogen Original Research Article, Wear, Volume 269, Issues 3–4, (2010) 229-240

[26] S. Hatami, L. Nyborg, L.O. Krona, Wear mechanisms of tool steels used in PM pressing dies, in: 2008, MPIF, Washington DC, USA.

[27] B. Bushan, Introduction to Tribology, John Wiely & Sons 2002.

[28] A. Magneli Structures of the ReO_3 -type with recurrent dislocations of atoms: ''Homologous Series'' of molybdenum and tungsten oxides, Acta Crystallographic 6 (1953) 495-500.

[29] U. Schwingenschögl, V. Eyert, The vanadium Magneli phasesV_nO_{2n-1}, Annalen der Physik 9 (13) (2004) 475-510.

[30] S. Andersson, A. Magneli, Diskrete titanoxydphasen im zusammensetzungsbereich TiO_1, $75 - TiO_{1.90}$, Die Naturwissenschaften 43 (21) (1956) 495-496.

[31] A.S.M. Woydt, I. Dörfel, K. Witke, Wear engineering oxides/anti-wear oxides, Wear 218 (1998) 84-95.

[32] A. Magneli, Structural order and disorder in oxides of transition metals of the titanium, vanadium and chromium groups chemistry of extended defects in non-metallic solids, in: Proc Inst for Advanced Study, 1969, pp. 148-162.

[33] G.Gassner, P.H. Mayerhofer, K. Kutschej, C. Mitterer, M. Kathrein, A new low friction concept for high temperatures: lubricious oxide formation on sputtered VN coatings, Tribology Letters 17 (4) (2004) 751-756.

[34] P.H. Mayrhofer , P.E. Hovsepian, C. Mitterer, W.-D. Munz, Calorimetric evidence for frictional self-adaption of TiAlN/VN superlattice coatings, surface and Coatings Technology 177-178 (2004) 341-347.

[35] P.E. Hovsepian, W.-D. Munz, Recent progress in large-scale production of nanoscale multilayer/superlattice hard coatings, Vaccum 69 (2003) 27-36.

[36] A. Glaser, S. Surnev, F.P. Netzer, N. Fateh, G.A. Fontalvo, C. Mitterer, Oxidation of vanadium nitride and titanium nitride coatings, Surface Science 601 (2007) 1153-1159.

[37] H.So*, D.S. Yu, C.Y.Chaung. Formation and wear mechanism of tribo-oxides and the regime of oxidational wear of steel; (2002)